Systematically improvable mean-field variational ansatz for strongly correlated systems: Application to the Hubbard model

Sandro Sorella*
SISSA—International School for Advanced Studies, Via Bonomea 265, 34136 Trieste, Italy
and Computational Materials Science Research Team, RIKEN Center for Computational Science (R-CCS), Kobe, Hyogo 650-0047, Japan

(Received 24 January 2021; revised 15 February 2023; accepted 21 February 2023; published 15 March 2023)

A systematically improvable wave function is proposed for the numerical solution of strongly correlated systems. With a stochastic optimization method, based on the auxiliary field quantum Monte Carlo technique, an effective temperature T_{eff} is defined, probing the distance of the ground-state properties of the model in the thermodynamic limit from the ones of the proposed correlated mean-field ansatz. In this way, their uncertainties from the unbiased zero temperature limit may be estimated by simple and stable extrapolations well before the so-called sign problem gets prohibitive. At finite T_{eff}, the convergence of the energy to the thermodynamic limit is indeed shown to already be possible in the Hubbard model for relatively small square lattices with linear dimension $L \simeq 10$, thanks to appropriate averages over several twisted boundary conditions. Within the estimated energy accuracy of the proposed variational ansatz, two clear phases are identified, as the energy is lowered by spontaneously breaking some symmetries satisfied by the Hubbard Hamiltonian: (a) a stripe phase where both spin and translation symmetries are broken and (b) a strong coupling d-wave superconducting phase when the particle number is not conserved and global $U(1)$ symmetry is broken. On the other hand, the symmetric phase is stable in a wide region at large doping and small coupling.

DOI: 10.1103/PhysRevB.107.115133

I. INTRODUCTION

The accurate numerical solution of the Schrödinger equation, namely, determining the ground state of a many-body Hamiltonian H, remains the most challenging unsolved problem since Dirac's formulation in 1931. Historically, important progress, with optimistic promise, occurs periodically, e.g., with the development of the density functional theory [1], the density matrix renormalization group (DMRG) [2,3], and its translation within the tensor network quantum information language [4–6], quantum Monte Carlo (QMC) methods [7–12], systematically improvable wave functions (WFs) based on multireference expansions [13–15], and machine-learning approaches [16,17], etc. However, apart from particular cases—as in one dimension [18] or for very particular couplings [19]—determining the exact ground state of a strongly correlated Hamiltonian H in the thermodynamic limit remains an open issue and a challenge for theoretical physicists. Also, for this reason, the Hubbard model has been historically used to benchmark unique techniques because its simplicity represents an ideal playground for advanced computational and experimental methods such as optical lattices [20].

Despite great theoretical effort, many of the properties of the 2D Hubbard model are still unclear [21,22]. Among the results that have been established by unbiased numerical techniques, it is well-known that an antiferromagnetic phase emerges at the half filling of the square lattice [8,23,24]. Away from half filling, the situation is less clear, although there is strong evidence that magnetic order remains [25]: the added holes (unoccupied sites) are expelled from the antiferromagnetic phase and essentially fill in equally spaced vertical lines of the lattice—the stripe phases. On the other hand, the quest for the occurrence of superconductivity in the Hubbard model has been highly debated and controversial since the discovery of high-temperature superconductivity [26–29].

Within this context, one of the clearest evidence of superconductivity was reported in the strong coupling limit of the Hubbard model, in the so-called $t-J$ model. Several years ago, this model was investigated in Ref. [30], within an almost standard variational Monte Carlo method (VMC) [31], whose main result was that superconductivity did not need electron-phonon interaction, but the driving force was rather the superexchange spin interaction J. The approach, and especially the claim, has been highly debated and is nowadays still controversial; nevertheless, it is worth mentioning that Corboz *et al.* [32] reported, by using tensor network, similar values for the off-diagonal d-wave superconducting long range order [33].

Despite this success, standard VMC based on a single reference mean-field ansatz, corrected by a simple correlation term (e.g., the Gutzwiller factor) is certainly limited as compared to the most recent and advanced variational methods that allow a systematically improvable ansatz. In view of this, in this paper, a different strategy is proposed to overcome the limitations of correcting a simple mean-field ansatz for reaching accurate ground-state properties. The approach will be dubbed in the following variational auxiliary field quantum Monte Carlo (VAFQMC), taking advantage

*Deceased.

of the enormous progress done in the last decades by two old but well-established techniques: the variational quantum Monte Carlo (VMC) and the auxiliary field quantum Monte Carlo (AFQMC) [9,10,34–36]. As for the former technique, we leverage its simplicity and clarity in interpreting the results in the thermodynamic limit, as well as its ability to optimize a mean-field state $|\psi_{\rm MF}\rangle$ in presence of a simple correlated factor. On the other hand, from AFQMC, a systematically convergent and nonperturbative expression of the correlation term is used, as AFQMC allows the application of the projection $\exp(-H\tau/2)$ to any mean-field state, filtering out exactly the ground-state component of $|\psi_{\rm MF}\rangle$ for large imaginary time τ. Therefore, and briefly speaking, the proposed VAFQMC takes the formalism of the AFQMC to yield an ansatz $|\psi_\tau\rangle_0 = \exp(-H\tau/2)|\psi_{\rm MF}\rangle$, which represents a systematically improvable—with increasing τ—correlated mean-field ansatz, retaining all advantages of the two mentioned formalisms.

The simple working hypothesis of this paper is the following. Suppose that, in the thermodynamic limit, the mean-field WF has acquired the lowest possible energy upon breaking some symmetry of the Hamiltonian in the presence of an accurate enough correlation term. In this case, the implicit VMC assumption is that the exact ground state should eventually show this phase. On the other hand, with the proposed method one can, in principle, tune the accuracy of the electron correlation at the desired level and verify explicitly the systematic evolution of the phase diagram, derived in this way, from the simplest mean-field Hartree-Fock (HF) theory ($\tau = 0$) to the converged projected one.

The paper is organized as follows. In Sec. II, we present the model and discuss the main features of the trial WF, while the details behind the Monte Carlo sampling and minimization of the energy are left to Sec. III. In Sec. IV, a benchmark for VAFQMC is presented, with the results away from half filling being discussed in Secs. V and VI. Our main conclusions are then summarized in Sec. VII.

II. MODEL AND WAVE FUNCTION

A. The ansatz

In this paper, we investigate the repulsive Hubbard model, whose Hamiltonian reads

$$H = -t\sum_{\langle \mathbf{i},\mathbf{j}\rangle,\sigma}(c^\dagger_{\mathbf{i}\sigma}c_{\mathbf{j}\sigma} + \text{H.c.}) - \mu\sum_{\mathbf{i},\sigma} n_{\mathbf{i},\sigma} + U\sum_{\mathbf{i}} n_{\mathbf{i},\uparrow}n_{\mathbf{i},\downarrow}, \tag{1}$$

where the sums run over sites of the square lattice, with $\langle \mathbf{i},\mathbf{j}\rangle$ denoting nearest-neighbor sites under twisted boundary conditions. In Eq. (1), we use the second quantization formalism, with $c^\dagger_{\mathbf{i}\sigma}$ ($c_{\mathbf{i}\sigma}$) being creation (annihilation) operators of electrons on a given site $\mathbf{i}$, and spin σ, while $n_{\mathbf{i}\sigma} \equiv c^\dagger_{\mathbf{i}\sigma}c_{\mathbf{i}\sigma}$ are number operators. The first two terms on the right-hand side of the Hamiltonian correspond to the hopping of fermions and the chemical potential μ, respectively, with the latter determining the filling of the bands. The third term describes the local repulsive interaction between fermions, with coupling strength U. Hereafter, we define the lattice constant as unity, and the hopping integral t as the energy scale.

To facilitate the following discussion, we define $H = K_\mu + V$, with K_μ denoting the kinetic and chemical potential terms, while $V \equiv U\sum_i n_{i,\uparrow}n_{i,\downarrow}$ being the interacting one. Given this, we introduce the following ansatz [37–39]:

$$|\psi_\tau\rangle = \exp\left[-\frac{\tau}{2}(H_{\rm MF}(\boldsymbol{\alpha}) + V)\right]|\psi_{\rm MF}\rangle\,, \tag{2}$$

in which the bare kinetic energy operator in the projector $\exp(-H\tau/2)$ is generalized [i.e., $K_\mu \to H_{\rm MF}(\boldsymbol{\alpha})$], by allowing a generic operator quadratic in the fermion ones $c, c^\dagger$, but also including a set of new variational parameters α, e.g., as a d-wave Bardeen-Cooper-Schrieffer (BCS) pairing field. This approach shares some similarities with those in quantum computation [40,41], with the purpose to reach accurate ground-state properties in the shortest possible projection time τ. As discussed later, such a variational WF represents a straightforward improvement of the standard AFQMC one, $|\psi_\tau\rangle_0$, mentioned in the Introduction.

The mean-field WF $|\psi_{\rm MF}\rangle$ can be a generic quasi-free-electron state, from a simple Slater determinant to BCS pairing functions, including singlet and/or triplet correlations. Here, $|\psi_{\rm MF}\rangle$ is allowed, breaking some symmetries of the Hamiltonian, and is defined as the ground state of a mean-field Hamiltonian $H_{\rm MF}(\boldsymbol{\alpha_0})$, i.e., $H_{\rm MF}(\boldsymbol{\alpha_0})|\psi_{\rm MF}\rangle = E_0(\boldsymbol{\alpha_0})|\psi_{MF}\rangle$, with a set of variational parameters indicated by the vector $\boldsymbol{\alpha_0}$.

For the projection operator, we take advantage of the variational formulation, so any extension of the variational ansatz containing $|\psi_\tau\rangle_0$ as a particular case should necessarily improve it; i.e., after energy optimization, it acquires a lower variational energy. Therefore, as discussed above, the bare kinetic energy operator in $\exp(-H\tau/2)$ is generalized [i.e., $K_\mu \to H_{\rm MF}(\boldsymbol{\alpha})$], with $H_{\rm MF}(\boldsymbol{\alpha})$ being parametrized by a set of variational parameters indicated by another independent vector $\boldsymbol{\alpha}$, such that one obtains $H_{\rm MF}(\boldsymbol{\alpha}) = K_\mu$ when $\boldsymbol{\alpha} = 0$. In other words, the key idea is that if a symmetry is broken in the thermodynamic limit, also the projection operator (i.e., the correlation factor), and not only the mean-field state $|\psi_{\rm MF}\rangle$, may break the symmetry and therefore $H_{\rm MF}(\boldsymbol{\alpha})$ is conveniently parametrized in a way similar to $\psi_{\rm MF}$.

This original formulation improves the quality of the ansatz and the smooth convergence to the thermodynamic limit as compared to the simpler ansatz $|\psi_\tau\rangle_0$, with the optimal energy being obtained after the simultaneous optimization of both $\boldsymbol{\alpha}$ and $\boldsymbol{\alpha_0}$. At this point, we anticipate that, in this variational formulation of VAFQMC, τ plays the role of an effective inverse temperature that is kept fixed during the minimization of the energy expectation value for the corresponding $|\psi_\tau\rangle$.

The optimization techniques known in standard VMC [42] and machine learning [43] will be generalized here to AFQMC. Before that, it is worth emphasizing simple but important properties of this ansatz:

(1) It is systematically improvable. To realize this property, it is enough to take $\boldsymbol{\alpha} = 0$ when the proposed ansatz coincides with the simpler one, $|\psi_\tau\rangle_0 = \exp(-H\tau/2)|\psi_{\rm MF}\rangle$. Thus, let $\tau \to \infty$ for a mean field $|\psi_{\rm MF}\rangle$ of the chosen form that is not orthogonal to the ground state. In this limit, $|\psi_\tau\rangle_0$ is obviously converging to the exact ground state. Thus, after turning on optimization, by allowing both $\boldsymbol{\alpha} \neq 0$ and, independently, $\boldsymbol{\alpha_0}$ different from the initial guess, a lower energy

is necessarily implied for each τ, yielding that the ansatz of Eq. (2) is systematically improvable, as well as being even better than $|\psi_\tau\rangle_0$ as far as its energy is concerned.

(2) It is size extensive. As discussed in Ref. [34], the WF is defined directly in terms of an exponential of an extensive operator, hence the statement. In practice, this means that, at a given τ, approximately the same accuracy for intensive quantities is expected, e.g., the energy per site or bulk correlation functions.

(3) For finite clusters, the convergence is exponential in τ due to the finite size gap between the ground-state manifold (which may be also degenerate) and the first excitation with nonzero energy gap. However, in the thermodynamic limit, this gap is probably always vanishing in this model, even for the half-filled insulator, where gapless spin-wave excitations are expected due to the occurrence of antiferromagnetic order for any $U > 0$ [23]. This situation, as will be shown in the following, makes the extrapolation to the unbiased limit, $\frac{1}{\tau} \to 0$, much simpler than the corresponding finite size case. Indeed, this can be obtained by simple and stable low-order polynomial extrapolations in something that can be considered an effective temperature $T_{\text{eff}} = 1/\tau$.

At this point, it is worth mentioning that, in the VAFQMC, the choice of the mean-field WF, as well as the ansatz of the projection operator–$K_\mu \to H_{\text{MF}}$ in the $\exp(-\frac{\tau}{2}H)$ operator—may affect the convergence toward the ground state. Indeed, we have noticed that the inclusion of this new set of variational parameters (from the ansatz of the projection operator) leads to a faster convergence, which, in turn, does not require long imaginary times to reach the ground state, in contrast with the regular AFQMC methods. Although a formal analytical demonstration of such a faster convergence is not provable at present time, one may appreciate it *a posteriori*, from the following results presented in this paper, which are in very good agreement with the best benchmarks provided in the literature, even to small values of imaginary times.

B. The $T_{\text{eff}} \to 0$ extrapolation

Therefore, the first step of this work is to converge results to the thermodynamic limit with large enough cluster size simulations and appropriate boundary conditions. Given this, simple and stable extrapolations for $T_{\text{eff}} \to 0$ are employed, thus achieving, with this strategy, very accurate results, or at least an estimate of the accuracy of the lowest T_{eff} variational ansatz. As presented later, this is often possible because, after the optimization, the physical properties of the ansatz [Eq. (2)] are already in the very low temperature regime, where the mentioned extrapolations are indeed stable and reliable within a given broken symmetry phase.

It is well established [44–46] that, when a standard type of order that breaks a continuous symmetry sets in, the corresponding gapless low energy excitations—i.e., typically bosons with a density of states $\rho(\epsilon) \propto \epsilon^{D-1}$–induce $\simeq T^3$ energy corrections in the limit $T \to 0$ for 2D, or $\simeq T^2$ ones for quasi-1D systems (as finite cylinder with infinite length). Due to these corrections, $\Delta E \propto \int_0^T \epsilon\rho(\epsilon) \simeq T^{D+1}$, it turns out that the fit

$$E(T_{\text{eff}}) = E(0) + aT_{\text{eff}}^{D+1} + bT_{\text{eff}}^{D+2} \tag{3}$$

is generally very appropriate for the systems studied here because the available T_{eff} always appear quite close to the correct asymptotic behavior. A formal derivation of the finite effective temperature corrections is outlined in Appendix A.

C. Boundary conditions and Trotter decomposition

Given the above arguments, particularly useful boundary conditions are adopted such that the convergence to the thermodynamic limit at fixed τ is as fast as possible. To this end, twisted averaged boundary conditions (TABCs) [47,48] are used in both the Hubbard Hamiltonian and the mean-field ones on rectangular $L_x \times L_y$ clusters ($L_x = L_y = L$ is adopted for square lattices). This is obtained by imposing opposite twists for opposite spins:

$$\begin{aligned} c_{r_x+L_x,r_y,\uparrow} &= c_{r_x,r_y,\uparrow}\exp(i2\pi\theta_x),\\ c_{r_x,r_y+L_y,\uparrow} &= c_{r_x,r_y,\uparrow}\exp(i2\pi\theta_y),\\ c_{r_x+L_x,r_y,\downarrow} &= c_{r_x,r_y,\downarrow}\exp(-i2\pi\theta_x),\\ c_{r_x,r_y+L_y,\downarrow} &= c_{r_x,r_y,\downarrow}\exp(-i2\pi\theta_y), \end{aligned} \tag{4}$$

with $\theta_x = -1/2 + (i-1/2)/N_T$ and $\theta_y = -1/2 + (j-1/2)/N_T$ for integers $1 \leqslant i, j \leqslant N_T$, while r_x and r_y here and henceforth indicate integer Cartesian coordinates of the lattice $1 \leqslant r_x \leqslant L_x$, $1 \leqslant r_y \leqslant L_y$. All the results are then averaged on a mesh of $N_T \times N_T$ twists in the Brillouin zone (BZ), with N_T large enough to have converged energies within statistical errors. When H_{MF} conserves the number of particles N and has a gap in the one particle spectrum, N remains unchanged for each twist, whereas when a BCS pairing is present, grand canonical ensemble is adopted as discussed in Ref. [49] and the expectation value of $H - \mu\hat{N}$ is minimized by the proposed variational ansatz, where $\hat{N} = \sum_{r_x,r_y,\sigma} c^\dagger_{r_x,r_y,\sigma} c_{r_x,r_y,\sigma}$ is the particle number operator.

It is worth remarking that the use of opposite twists for opposite spin electrons is particularly important in this case because it allows the conservation of the translation symmetry in the BCS mean-field Hamiltonian, at least in a simple way.

Before explaining how to optimize the variational parameters, it is useful to appreciate in Fig. 1 the fast and smooth convergence of the grand potential $\Omega = \frac{\langle\psi_\tau|H-\mu\hat{N}|\psi_\tau\rangle}{\langle\psi_\tau|\psi_\tau\rangle}$ in the thermodynamic limit as a function of the number N_s of sites for a value of the chemical potential corresponding to doping $\delta = 1 - N/N_s \approx 1/8$.

The other important ingredient for an efficient implementation of Eq. (2) is the use of a particularly suited Trotter decomposition for the corresponding propagator:

$$\begin{aligned} &\exp\left[-\frac{\tau}{2}(H_{\text{MF}}(\boldsymbol{\alpha}) + V)\right]\\ &\quad= \left\{\prod_{i=1}^{n} \exp\left[-t_i H_{\text{MF}}(\boldsymbol{\alpha})\right]\exp\left[-h_i V\right]\right\}\\ &\qquad\times \exp\left[-t_{n+1}H_{\text{MF}}(\boldsymbol{\alpha})\right], \end{aligned} \tag{5}$$

where, in principle, h_i and t_i can be independently optimized to minimize the Trotter error, as proposed in a recent work [40]. Henceforth, it is assumed that the operators in Eq. (5) are ordered from left to right according to increasing values of the integer i. In this paper, τ is kept fixed, and therefore the

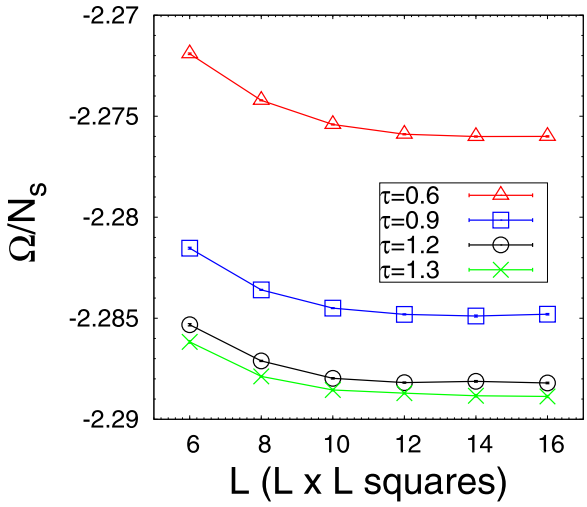

FIG. 1. Grand potential per site Ω/N_s as a function of cluster size for different values of the projection time τ for $\mu = 1.75t$ and $U/t = 8$.

following constraint is imposed:

$$\sum_{i=1}^{n} h_i = \frac{\tau}{2}. \tag{6}$$

Moreover, to minimize the number of variational parameters and the number n, the following parametrization is adopted:

$$h_i = \Delta\tau\gamma^{i-1}, \tag{7}$$

$$t_i = \frac{h_i + h_{i-1}}{2} \text{ for } i = 1, 2, \cdots n, \tag{8}$$

with $h_0 = 0$ and $\gamma > 1$ chosen in a way to satisfy the constraint in Eq. (6). This expression is based on the conventional small $\Delta\tau$ symmetric Trotter decomposition $\exp[-\Delta\tau(H_{\rm MF}(\boldsymbol{\alpha}) + V)] = \exp[-\frac{\Delta\tau}{2}H_{\rm MF}(\boldsymbol{\alpha})]\exp[-\Delta\tau V]\exp[-\frac{\Delta\tau}{2}H_{\rm MF}(\boldsymbol{\alpha})] + O(\Delta\tau^3)$, where a nonuniform time step according to Eq. (7) has been chosen because, for high accuracy, it is important only that the first time step is small and $\gamma \simeq 1$. In this way, the efficiency and the number of operators involved is significantly optimized, without using too many variational parameters, as in Ref. [40]. In all forthcoming calculations, only a single parameter $\Delta\tau$ is optimized with the convenient choice

$$n = \text{Max}\{[(\tau U/0.4 - 1)/5], 1\}, \tag{9}$$

leading to a Trotter time step error on the energy that, for all U values reported, is comparable to, or less than, the statistical errors from the Monte Carlo sampling. Here and henceforth, the square brackets indicate the integer part of a real number.

III. VARIATIONAL AUXILIARY FIELD METHOD

A. The auxiliary fields

Since $H_{\rm MF}(\boldsymbol{\alpha})$ is a one-body operator and $|\psi_{\rm MF}\rangle$ is a mean-field state (e.g., a Slater determinant) there is no difficulty to apply $\exp[-t_i H_{\rm MF}(\alpha)]$ to $|\psi_{\rm MF}\rangle$. Moreover, taking into account that $\exp[-t_i H_{\rm MF}(\alpha)|\psi_{\rm MF}\rangle$ remains a mean-field state, this operation can be also performed iteratively.

The application of $\exp(-h_i V)$ is instead more complicated, and can nevertheless be implemented by using the auxiliary fields technique. For this purpose, the following discrete Hubbard-Stratonovich transformation [8] is used:

$$\exp(-h_i V) = 2^{-N_s}\exp(-U h_i \hat{N}/2)\sum_{\sigma_{j,i}=\pm 1}\exp(\lambda_i\sum_j \sigma_{ji} m_j), \tag{10}$$

with $m_j = n_{j,\uparrow} - n_{j,\downarrow}$, $\hat{N}$ being the total number of particles operator, $\cosh\lambda_i = \exp(U h_i)$, and $\sigma_{ji} = \pm 1$ being auxiliary fields for each site j of the lattice, and Trotter slice i. Notice that the factor $\exp(-U h_i \hat{N}/2)$ represents only an irrelevant change of the chemical potential in $H_{\rm MF}(\boldsymbol{\alpha})$, and will therefore be omitted for simplicity here and henceforth.

B. Expectation values

Within this setting, the expectation value of the Hamiltonian H (or any relevant correlation function [50]) for the WF in Eq. (2) is given by

$$\begin{aligned} E_n &= \frac{\langle\psi_n|H|\psi_n\rangle}{\langle\psi_n|\psi_n\rangle} \\ &= \frac{\sum_{\sigma\sigma'}\langle\psi_{\rm MF}|U_n^\dagger(\boldsymbol{\sigma'})H U_n(\boldsymbol{\sigma})|\psi_{\rm MF}\rangle}{\sum_{\sigma\sigma'}\langle\psi_{\rm MF}|U_n^\dagger(\boldsymbol{\sigma'})U_n(\boldsymbol{\sigma})|\psi_{\rm MF}\rangle}, \end{aligned} \tag{11}$$

where $\boldsymbol{\sigma}$ indicates the $N_s \times n$-dimensional vector with components σ_{ji}, and

$$\begin{aligned} U_n(\boldsymbol{\sigma}) = &\exp[-H_{\rm MF}(\boldsymbol{\alpha})t_1]\exp\left[\lambda_1\sum_j \sigma_{j,1}m_j\right]\cdots \\ &\exp[-H_{\rm MF}(\boldsymbol{\alpha})t_n]\exp\left[\lambda_n\sum_j \sigma_{j,n}m_j\right] \\ &\exp[-H_{\rm MF}(\boldsymbol{\alpha})t_{n+1}]. \end{aligned} \tag{12}$$

Therefore, one may perform a sampling of the Ising auxiliary fields $\boldsymbol{\sigma}$ and $\boldsymbol{\sigma'}$ by standard Monte Carlo methods, according to the weight $|W_n(\boldsymbol{\sigma'}, \boldsymbol{\sigma})|$, where

$$W_n(\boldsymbol{\sigma'}, \boldsymbol{\sigma}) = \langle\psi_{\rm MF}|U_n^\dagger(\boldsymbol{\sigma'})U_n(\boldsymbol{\sigma})|\psi_{\rm MF}\rangle. \tag{13}$$

Generally, in the complex case, W_n has a nontrivial phase that is determined by $S_n(\boldsymbol{\sigma'}, \boldsymbol{\sigma}) = \frac{W_n(\boldsymbol{\sigma'},\boldsymbol{\sigma})}{|W_n(\boldsymbol{\sigma'},\boldsymbol{\sigma})|}$, a complex number with unit modulus, that plays the role of the infamous fermionic minus-sign problem in QMC methods.

Finally, E_n can be computed by

$$E_n = \frac{\sum_{\sigma\sigma'}|W_n(\boldsymbol{\sigma'}, \boldsymbol{\sigma})|e_n(\boldsymbol{\sigma'}, \boldsymbol{\sigma})S_n(\boldsymbol{\sigma'}, \boldsymbol{\sigma})}{\sum_{\sigma\sigma'}|W_n(\boldsymbol{\sigma'}, \boldsymbol{\sigma})|S_n(\boldsymbol{\sigma'}, \boldsymbol{\sigma})} \tag{14}$$

by evaluating the ratio of the means corresponding to two real random variables, $\text{Re}[e_n(\boldsymbol{\sigma'}, \boldsymbol{\sigma})S_n(\boldsymbol{\sigma'}, \boldsymbol{\sigma})]$ and $\text{Re}[S_n(\boldsymbol{\sigma'}, \boldsymbol{\sigma})]$ [51], over the configurations generated by Monte Carlo sampling, according to the probability $p_n(\boldsymbol{\sigma'}, \boldsymbol{\sigma}) = \frac{|W_n(\boldsymbol{\sigma'},\boldsymbol{\sigma})|}{\sum_{\sigma\sigma'}|W_n(\boldsymbol{\sigma'},\boldsymbol{\sigma})|}$, and by using the standard technique described in Ref. [34].

Here,

$$e_n(\boldsymbol{\sigma}', \boldsymbol{\sigma}) = \frac{\langle \psi_{\mathrm{MF}} | U_n^\dagger(\boldsymbol{\sigma}') H U_n(\boldsymbol{\sigma}) | \psi_{\mathrm{MF}} \rangle}{W_n(\boldsymbol{\sigma}', \boldsymbol{\sigma})} \tag{15}$$

is a sort of local energy, namely, an estimate of E_n for a given configuration of the Ising fields $\boldsymbol{\sigma}$ and $\boldsymbol{\sigma}'$. Indeed, both $e_n(\boldsymbol{\sigma}', \boldsymbol{\sigma})$ and $S_n(\boldsymbol{\sigma}', \boldsymbol{\sigma})$, as well as $W_n(\boldsymbol{\sigma}', \boldsymbol{\sigma})$, can be computed in $\propto N_s^3 n$ operations because they involve essentially imaginary time propagations of mean-field states under time-dependent one-body propagators $U_n(\boldsymbol{\sigma})$ and $U_n(\boldsymbol{\sigma}')$.

C. Energy derivatives

The basic ingredient introduced in this paper is the possibility to compute energy derivatives of E_n with respect to all the parameters defining the WF, i.e., $\boldsymbol{\alpha}$ and $\boldsymbol{\alpha}'$, henceforth assumed to be defined by the $2p$ variational parameters $\alpha_1, \alpha_2, \cdots \alpha_{2p}$ and the minimum time step used $\Delta\tau = \alpha_{2p+1}$ at fixed τ, according to Eq. (6). Simple algebraic computations, very similar to the ones known for VMC, imply that any energy derivative $\frac{\partial E_n}{\partial \alpha_j}$ with respect to an arbitrary variational parameter α_j, for $j = 1, 2, \cdots 2p+1$, can be computed by means of corresponding derivatives of two complex functions $\frac{\partial e_n}{\partial \alpha_j}$, $O_j = \frac{\partial \ln(W_n)}{\partial \alpha_j} = \frac{\partial W_n}{\partial \alpha_j}/W_n$ of the local energy and the logarithm of the weight, respectively,

$$\frac{\partial E_n}{\partial \alpha_j} = \frac{\langle\langle \mathrm{Re}\left\{ S_n \left[\frac{\partial e_n}{\partial \alpha_j} + (e_n - E_n) O_j \right] \right\} \rangle\rangle}{\langle\langle \mathrm{Re}(S_n) \rangle\rangle}, \tag{16}$$

where here and henceforth the symbol $\langle\langle * \rangle\rangle$ indicates the average of the generic random variable $*$ over the probability distribution p_n defined before, and for shorthand notations the dependence on $\boldsymbol{\sigma}$ and $\boldsymbol{\sigma}'$ of all the quantities involved is not explicitly shown.

The differentiation of the complex quantities $\ln W_n$ and e_n, required for the $\frac{\partial E_n}{\partial \alpha_j}$ evaluation, at given values of $\boldsymbol{\sigma}$ and $\boldsymbol{\sigma}'$, may appear very cumbersome and involved especially considering that, it is often necessary, as in VMC, to optimize several parameters. This task can be easily achieved in a computational time equal to the one required to compute the complex quantities $\ln(W_n)$ and e_n, remarkably only up to a small prefactor regardless of how large the number of variational parameters involved. This is possible by using adjoint algorithmic differentiation [52], a technique that is becoming popular in the field of machine learning with another name, i.e., back propagation, but was certainly known before in applied mathematics [53], and only recently has been appreciated in physics [54,55]. Once all energy derivatives $\partial_j E$ are known, the usual scheme adopted in VMC can also be applied here. Variational parameters are changed according to the equation

$$\delta\boldsymbol{\alpha} = -\mathrm{rate}_{\mathrm{learning}} F^{-1} \frac{\partial E}{\partial \boldsymbol{\alpha}}, \tag{17}$$

where $\mathrm{rate}_{\mathrm{learning}}$ is a suitable small constant, determining the speed of convergence to the minimum and F is the so-called Fisher-information matrix, given by

$$F_{ij} = \left\langle\left\langle \frac{\partial \log p_n}{\partial \alpha_i} \frac{\partial \log p_n}{\partial \alpha_j} \right\rangle\right\rangle = \langle\langle \mathrm{Re}(O_i) \Re(O_j) \rangle\rangle\rangle \tag{18}$$

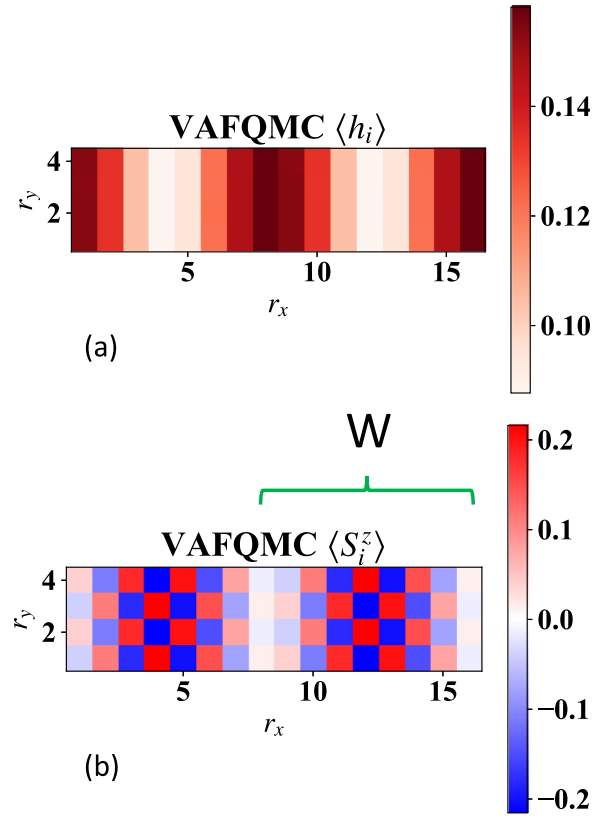

FIG. 2. Hole density (a) and spin density (b) for the stripe of width $W = 8$ and $U/t = 8$ for the 4×16 cluster obtained by energy optimization at $\tau t = 1.5$. The green bracket emphasizes the length W of the stripe, i.e., the distance between two domain walls.

where the symbol $\langle\langle\langle AB \rangle\rangle\rangle = \langle\langle AB \rangle\rangle - \langle\langle A \rangle\rangle\langle\langle B \rangle\rangle$ here indicates the covariance of two random variables over the probability p_n. We adopt here $\mathrm{rate}_{\mathrm{learning}} \simeq 6$ and the same regularization with $\epsilon = 0.01$ described in Ref. [34] to avoid instabilities in the calculation of the inverse matrix. Typically, convergence is reached with a few hundreds iterations and variational parameters are averaged after convergence for about 50 steps.

IV. BENCHMARKING THE METHOD

In this section, the proposed method is tested against known benchmark results on infinite systems. Unfortunately, there are only a few results available in the thermodynamic limit, mainly limited to ground-state energies. Nevertheless, they are extremely relevant for a variational method because its predictions can be supported by a good estimate of the energy.

We start our tests of VAFQMC by fixing $U/t = 8$, at doping $\delta = 1/8$, and dealing with cylinders with finite width L_y and periodic boundary conditions (PBCs) in the short y direction. It allows us to compare our results with the very accurate ones determined by DMRG with open boundary conditions (OBCs) in the x direction, and extrapolated to the one-dimensional $L_x = \infty$ thermodynamic limit. As seen in Fig. 3, VAFQMC is in very good agreement with the known results for $L_y \leqslant 6$, especially when the $T_{\mathrm{eff}}^2 \to 0$ extrapolation

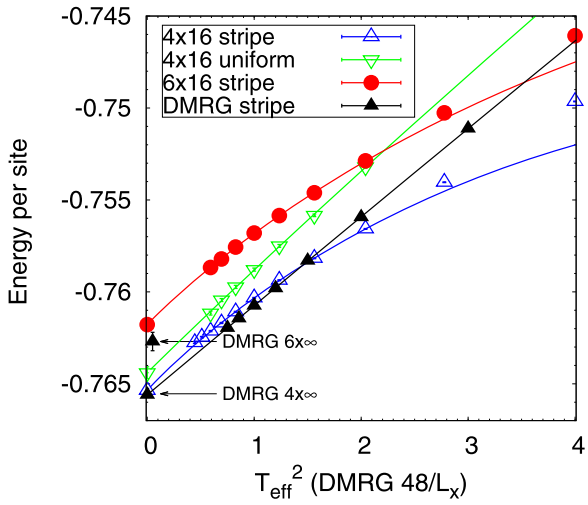

FIG. 3. Energy as a function of the effective temperature $T_{\rm eff} = 1/\tau$ for cylinders with different widths. Values at zero horizontal axis result from extrapolations. Here the $D = 1$ asymptotic form of Eq. (3) is adopted for the fit of the data in the range $0.7 \leqslant \tau t \leqslant 1.3$. This form is compatible with the expected low-energy spectrum (see text) while the range used is found to be appropriate for $U = 8t$ in all cases, including the 2D ones, studied in this paper. DMRG energies obtained with open boundary conditions are reported as a function of the inverse cylinder length L_x for the $4 \times L_x$ case, while the extrapolated ones at $L_x = \infty$ for both the $4 \times L_x$ and $6 \times L_x$ cases.

is employed in a relatively small $L_y \times 16$ cluster with 32 twists in the long direction [56]. This is remarkable because DMRG obviously has the best performance in quasi-1D systems. From Fig. 3, one may also notice the importance of using appropriate boundary conditions to reach the thermodynamic limit: OBCs require very large clusters for this end, which may make very accurate extrapolations a challenging issue. In addition to this, due to difficulties related to DMRG extrapolations when one approaches the 2D case, we expect that the small discrepancy between VAFQMC and DMRG extrapolated values for $L_y = 6$ does not necessarily imply that VAFQMC is less accurate in this case. As our partial conclusion, it is clear that the proposed extrapolations can be used to estimate the quality of the VAFQMC best (lowest $T_{\rm eff}$) variational energy estimates.

In all these VAFQMC calculations at doping $\delta = 1/8$, it has been found that the $W = 8$ stripe is the most favorable mean field, as shown in Fig. 2 for the $L_y = 4$ case. Here this state is parametrized by the most general mean-field Hamiltonian with local and nearest neighbor couplings independent of r_y (see also the Supplemental Material) [57]:

$$
\begin{aligned}
H_{\rm MF}(\boldsymbol{\alpha_0}) = & \sum_{r_x,r_y,\sigma} \left[-t_x(r_x) c^\dagger_{r_x+1,r_y,\sigma} c_{r_x,r_y,\sigma} \right. \\
& \left. - t_y(r_x) c^\dagger_{r_x,r_y+1,\sigma} c_{r_x,r_y,\sigma} + \text{H.c.} \right] \\
& + \sum_{r_x,r_y} \Delta_{\rm AF}(r_x) (-1)^{r_x+r_y} \left(n_{\uparrow,r_x,r_y} - n_{\downarrow,r_x,r_y} \right) \\
& - \mu(r_x) n_{r_x,r_y}, \qquad (19)
\end{aligned}
$$

where $n_{\uparrow,r_x,r_y} = c^\dagger_{\uparrow,r_x,r_y} c_{\uparrow,r_x,r_y}$, $n_{\downarrow,r_x,r_y} = c^\dagger_{\downarrow,r_x,r_y} c_{\downarrow,r_x,r_y}$, $n_{r_x,r_y} = n_{\uparrow,r_x,r_y} + n_{\downarrow,r_x,r_y}$. Thus, the local magnetic antiferromagnetic field satisfies $\Delta_{\rm AF}(r_x) = -\Delta_{\rm AF}(r_x + W)$ and the corresponding local chemical potential $\mu(r_x) = \mu(r_x + W)$. Moreover, nearest-neighbor hoppings $t_x(r_x) = t_x(r_x + W)$ and $t_y(r_x) = t_y(r_x + W)$ are also included, amounting to a total of $4W$ variational parameters defining $H_{\rm MF}(\boldsymbol{\alpha_0})$. All their values are assumed independent of the twists [49]. The few parameter choice adopted in Ref. [58] is used only to initialize the present more general $8W + 1$ (by including also the optimization of $H_{\rm MF}(\boldsymbol{\alpha})$ and $\Delta\tau$) parameter ansatz $|\psi_\tau\rangle$.

For the uniform solution (see Sec. VI) antiferromagnetic order is allowed only at half filling while at finite doping a four (three) parameter ansatz is adopted in $H_{\rm MF}(\boldsymbol{\alpha})$ ($H_{\rm MF}(\boldsymbol{\alpha_0})$, and $t = 1$ can be left unchanged, as it sets the scale of the mean-field energy, which is irrelevant for $|\psi_{\rm MF}\rangle$) including nearest- and next-nearest-neighbor hoppings and has a uniform chemical potential μ_0 and $d_{x^2-y^2}$ pairing. In all the following calculations, when the particle number is not defined, neither in the mean-field WF nor in the projection, the energy per site $e(\delta)$ at fixed doping δ is accurately estimated by an appropriate choice of the chemical potential μ. This is obtained by simple and stable interpolations with a few calculations in the grand canonical ensemble or, in other words, by inverting the Legendre transform from chemical potential dependence to the conjugate density one $1 - \delta$.

With this method, it is therefore possible to compute the energy in the thermodynamic limit of true 2D clusters without particular effort as the average (complex) sign $\langle\langle S_n \rangle\rangle$ is always larger than $\simeq 0.3$ for all the simulations reported in this paper. It is important to remark that, when the 2D-thermodynamic limit is approached, a small but systematic increase of the energy can be appreciated, confirming that to determine the correct two-dimensional thermodynamic limit, true 2D clusters have to be used.

For L_y small, the stripe solution is clearly favored as compared with the uniform solution, as found by DMRG. In Fig. 3, the uniform solution is optimized with a nonzero $d_{x^2-y^2}$ BCS pairing but remains clearly above the stripe solution even after extrapolation to $T_{\rm eff} = 0$.

However, the situation is quite different when the 2D thermodynamic limit is required. In this case, to compare the stripe with periodicity $W = 8$ and $W = 7$ and the uniform d-wave solution, calculations on a 16×16 and 14×16 clusters are carried out with 16×16 different twists in the BZ. For the d-wave ansatz, several calculations at different chemical potentials $\mu \simeq 1.8t$ are attempted to fulfill a doping $\delta = 1/8$ for each effective temperature $T_{\rm eff}$.

Figure 4 shows that in 2D the uniform solution turns out to have an energy competitive with the stripe ones, though the $W = 7$ stripe appears to also be the most stable solution because it always provides the lowest variational energy for each $T_{\rm eff}$. Nevertheless the stripe-uniform phase energy difference, reached at the lowest $T_{\rm eff}$ shown, is very small $\simeq 0.001t$, though the two variational states remain with qualitatively different types of correlation functions, i.e., a sizable magnetic moment in the former and non-negligible d-wave pairing correlations in the latter (see inset in Fig. 4). In Table I, the various extrapolated and best variational en-

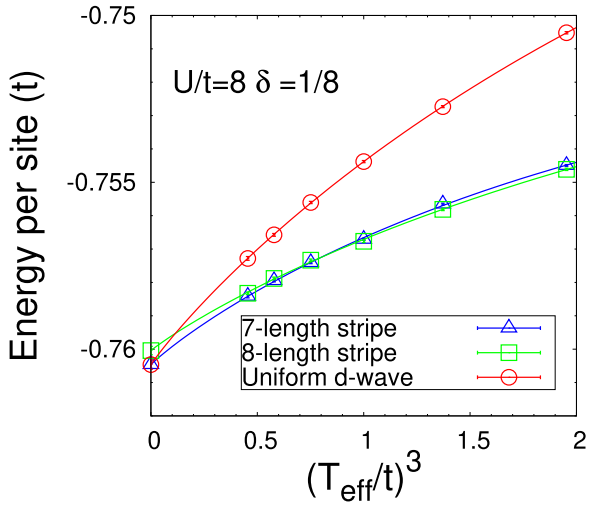

FIG. 4. Energy per site at doping $\delta = 1/8$ and $U/t = 8$ for the stripe solution of different lengths and the uniform d-wave superconducting one, corresponding to the same doping. Values at zero horizontal axis result from extrapolations. Here the $D = 2$ fitting form of Eq. (3) is adopted, which is compatible with the expected low energy spectrum (see text). A 16×16 square lattice was used for the $W = 8$ stripe and the uniform d-wave states while a 14×16 rectangular lattice for the $W = 7$ stripe. The inset shows the pairing correlations at maximum horizontal distance $L_x/2$.

ergies are compared with the available benchmark results [24,25,58] obtained with other variational methods. Remarkably, VAFQMC always provides the best-known variational energies in the thermodynamic limit. Here, for the VAFQMC, the results related to $4 \times \infty$, $16 \times \infty$, and $\infty \times \infty$ lattices correspond to 4×16, 6×16, and 16×16, respectively, with TABCs in the coordinates denoted by ∞ symbols. In 2D, the VAFQMC performances are manifestly excellent if compared with other variational methods because DMRG becomes rapidly inaccurate with increasing L_y and the best variational energy obtained by iPEPS is significantly higher than the VAFQMC one. This may explain why the iPEPS extrapolated energy has a large uncertainty and is much below the

TABLE I. Best variational energies and extrapolated energies (methods marked by *) for various methods as compared with VAFQMC (last rows) for the $U/t = 8$ Hubbard model at $\delta = 1/8$. The numbers in parenthesis represent error bars or uncertainties in the extrapolations in the last digit. Other quantum chemistry methods, also using multireference (MR) expansion, have shown "the need for a much larger MR expansion than that afforded" [24].

Method	$4 \times \infty$	$6 \times \infty$	$\infty \times \infty$
VMC+backflow [58]		−0.7483(1)	−0.74884(1)
DMRG* [25]	−0.76598(3)	−0.7627(5)	
DMRG* [60]	−0.7655(1)		
DMRG [60]	−0.761826		
iPEPS [61]			−0.75333
iPEPS* [25]			−0.767(2)
This paper	−0.76276(5)	−0.75867(3)	−0.75842(5)
This paper*	−0.7654(1)	−0.7618(1)	−0.7605(1)

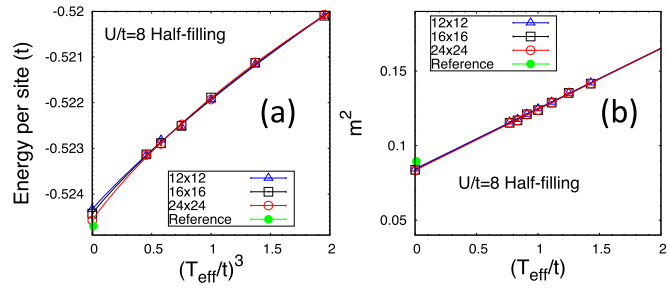

FIG. 5. Energy per site (a) and spin-spin correlation function at maximum distance (b) converging to the square antiferromagnetic order parameter m^2 in the thermodynamic limit. All calculations refer to half filling and are shown as a function of the effective temperature $T_{\text{eff}} = 1/\tau$. Values at zero horizontal axis result from extrapolations. The estimated exact reference values in the thermodynamic limit are taken from Ref. [24] for the energy and Ref. [23] for m.

VAFQMC and DMRG $6 \times \infty$ ones. It is also possible that the extrapolation in the bond dimension is quite inaccurate and can be substantially improved [59].

Finally, the energy and magnetic order parameter are compared at half filling. In this case, there is no sign problem and, in principle, large imaginary times can be employed without particular difficulties. However, $\tau t \leqslant 1.3$ has also been chosen in this case to show the strength of this approach even when short time projections are employed. For the order parameter, finite effective temperature scaling analysis implies convergence linear in T_{eff} much slower than the energy (see Appendix A). Nevertheless, remarkably accurate results can be obtained in both cases, as shown in Fig. 5. At finite effective temperature T_{eff}, very weak finite-size effects are seen, showing once more the great advantage of using TABCs with this approach. The error in the $T_{\text{eff}} \to 0$ extrapolated energy is then compatible with the reference one within the error bars [this paper, extrapolation $E_h = -0.52443(14)$, reference $-0.5247(2)$] whereas the extrapolated order parameter (0.2894(16)) is in very good agreement with the benchmark one [0.2991(2)].

V. THE HARTREE-FOCK STRIPE PHASE

Also within the HF method, namely, by considering a simple Slater determinant or also uncorrelated BCS mean-field WFs, very few established results are known, if we allow also nonuniform solutions [62,63], i.e., non-translation-invariant solutions with large unit cells. At half filling, it is clear that the simple antiferromagnetic solution, with two sites per unit cell, is stable for any $U > 0$ as has been shown analytically by Hirsch [8]. On the other hand, it is well-known that no superconducting solution is possible for $U > 0$. Restricting the solution to a small unit cell containing only two sites leads to a phase separation instability [64], namely, the energy per hole,

$$e_h(\delta) = \frac{(e(\delta) - e(0))}{\delta}, \tag{20}$$

acquires a minimum at a finite doping δ_c and for any doping $\delta \leqslant \delta_c$ it is more convenient to expel the holes from a pure antiferromagnet with energy per site $e(0)$ in a region with

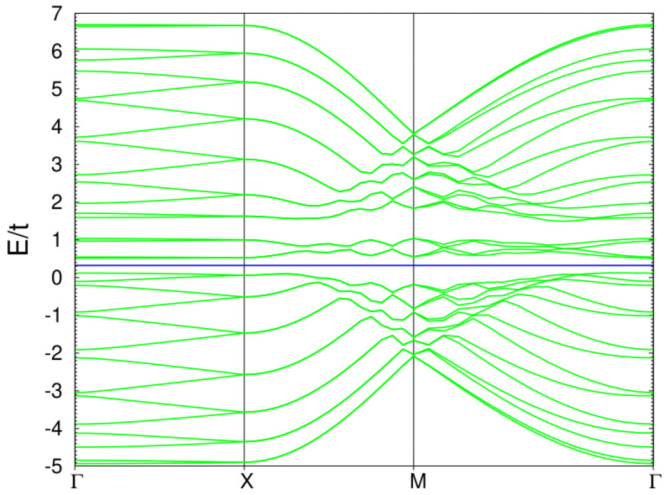

FIG. 6. Hartree-Fock bands for the $W = 8$ stripe at $U/t = 8$ and doping $\delta = 1/8$. There are 32 different bands and only the lowest energy 14 bands are completely occupied at this filling, implying insulating behavior, as the Fermi energy (blue line) clearly separates the lowest occupied bands from the empty ones. Here $\Gamma = (0, 0)$, $X = (\pi/16, 0)$ and $M = (\pi/16, \pi/2)$.

appropriate size containing an hole rich phase at doping δ_c. After this construction (see, e.g., Appendix B) $e_h(\delta)$ will be constant in the thermodynamic limit and equal to $e_h(\delta_c)$ for all dopings $\delta \leqslant \delta_c$. This represents a fingerprint of phase separation and the study of the energy per hole can also be considered an implicit way to build a nonuniform solution (when a minimum is found) within not only HF but any variational approach based on a translationally invariant ansatz.

However, a better way to expel holes from an antiferromagnet is found by means of the stripe solution already reported in Fig. 2. In particular, when the doping $\delta = 1/W$ the HF bands show a clear insulating behavior because the unit cell $2 \times 2W$ contains $4W$ doubly-degenerate bands [65] and $2W - 2$ are fully occupied, as is the case for $\delta = 1/8$ shown in Fig. 6. The insulating nature of this stripe solution was also pointed out in the weak coupling HF theory by Schulz [62] who discovered the stability of incommensurate magnetic states with finite wave vector $Q = (\pi \pm \pi\delta, \pi)$ close to the antiferromagnetic one $Q = (\pi, \pi)$, and the opening of a full gap away from half filling within HF. The occurrence of a finite gap in this case is easily understood not only because the mean-field HF Hamiltonian turns out to have a gap but also for the following simple general argument holding also in the correlated case. This incommensurate state is adiabatically connected to the insulator having equally spaced empty (i.e., with no electrons) vertical lines of sites separating half-filled antiferromagnetic insulating regions.

In this way, the HF solution can avoid phase separation but the corresponding energy per hole is almost flat at small doping [see Fig. 7(a)] that is almost equivalent to phase separation. Indeed, at small doping the stripes are very far apart $W = \frac{1}{\delta}$ and do not interact at all, as can be appreciated in Fig. 7(b), where the interaction between two vertical stripes at distance W is given by $I(W) = e_h(\delta = 1/W) - e_h(\delta = 1/\infty)$. $I(W)$ here defined represents the energy cost per hole

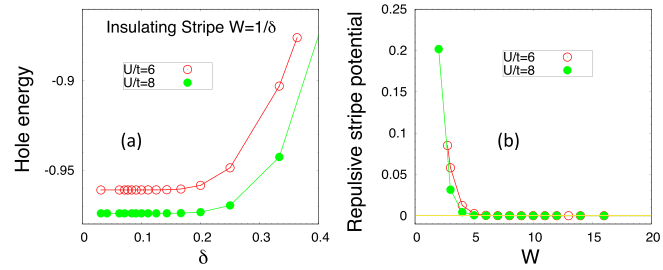

FIG. 7. Hole energy (a) for the stripe of width W commensurate with the doping δ within Hartree-Fock. The blue triangles for $U/t = 8$ correspond to intermediate dopings obtained by applying the composition rule described at the end of Sec. V. (b) Effective repulsion energy between equally spaced vertical stripes as a function of their distance W.

for two stripes being at finite distance W rather than at infinite distance, where they do not interact.

At noncommensurate doping, for instance, $1/8 < \delta < 1/7$, it is possible to verify that such kinds of insulating solutions at $\delta = 1/7$ and $\delta = 1/8$ can be joined together by forming a smooth doping-dependent insulating stripe phase at any intermediate doping [see, for instance, Fig. 7(a) for $U/t = 8$]. Many stripes at positions r_{x_i} of the lattice can be thought to interact by means of a pairwise repulsive interaction $\propto \sum_{i<j} I(r_{x_i} - r_{x_j})$, with interaction $I(W)$ as the one computed in Fig. 7(b). Thus, the rule for obtaining the minimum HF energy is as follows: To get the appropriate stripe for a given hole density δ, one may alternate/combine energetically more expensive stripes of length W smaller than $[1/\delta + 1]$ ($W = 7$ in this case) by placing them as far as possible.

VI. RESULTS FOR THE CORRELATED PHASE DIAGRAM

The rule determined in the previous section to identify the minimum energy insulating stripe solution has also been verified in the correlated case up to the maximum τ possible with essentially no sign problem, namely, $\tau t = 1.3, 1.73, 2.6$ for $U/t = 8, 6, 4$, respectively. Therefore, first the stripe WF (breaking translation and spin symmetry) is computed at commensurate doping $\delta = 1/W$, where W, being the distance between equally spaced stripes, is an integer. Then, to account for intermediate dopings, the corresponding energies are interpolated. Moreover, to estimate the error to the exact $T_{\text{eff}} = 0$ limit, the results are extrapolated to this limit. Hence, the lowest energy of the uniform solution is estimated that is parametrized by the following mean-field Hamiltonian:

$$H_{\text{MF}}(\boldsymbol{\alpha_0}) = \bar{K} - \mu_0 \hat{N} + \Bigg[\Delta_{\text{AF}} \sum_R (-1)^{r_x + r_y} c^\dagger_{R,\uparrow} c_{R,\downarrow} + 2\Delta_{x^2-y^2} \sum_k (\cos k_x - \cos k_y) c^\dagger_{k,\uparrow} c^\dagger_{-k,\downarrow} + \text{H.c.} \Bigg] \tag{21}$$

where $\bar{K} = \sum_{i,j,\sigma} t_{R,R'} c^\dagger_{R,\sigma} c_{R',\sigma}$ is the translation-invariant kinetic energy defined here by the nearest- and next-nearest-neighbor hoppings t and t', namely, $t_{R,R'} = -t$ ($t_{R,R'} = -t'$) if R and R' are (next) nearest neighbor sites, $\Delta_{x^2-y^2}$ determines

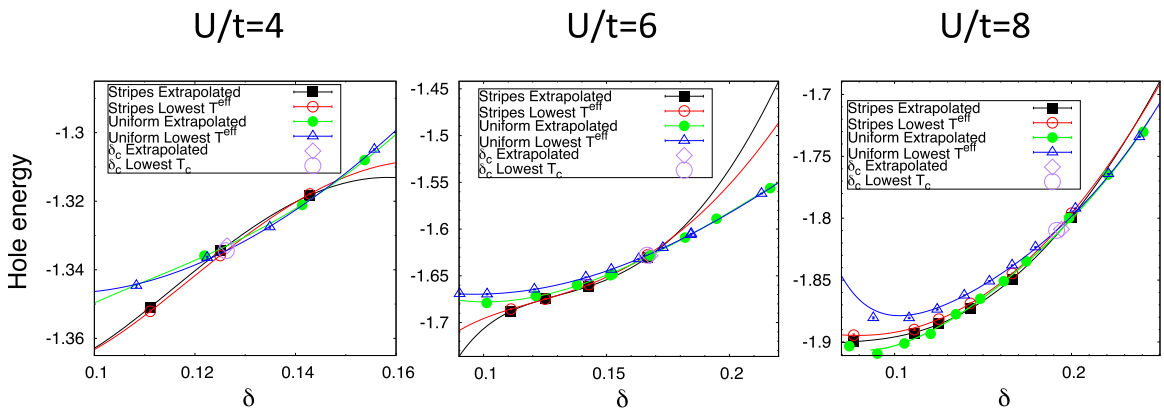

FIG. 8. Determination of the critical doping where the transition between the uniform phase and the stripe phase occurs with lower energy at small doping. The empty big dots (tilted squares) represent the transition points corresponding to the best variational estimates (extrapolated to zero temperature ones) at the lowest effective temperatures T_{eff}. Here, the chosen stripes are the $W = 1/\delta$ ones–notice that, in panel (c), the $W = 1/\delta$ stripe is not the one with lowest energy at low doping. See, e.g., Fig. 9.

the gap function for a $d_{x^2-y^2}$ BCS superconductor, Δ_{AF} is the mean-field gap due to a commensurate antiferromagnetic state, and μ_0 is the mean-field chemical potential value.

By the proposed energy optimization method, as the doping is decreased, clear evidence of an instability toward $d_{x^2-y^2}$ BCS pairing is found, because as soon as $\Delta_{x^2-y^2}$ turns out to be nonzero in the thermodynamic limit, the variational WF $|\psi_\tau\rangle$, breaks the $U(1)$ symmetry $c_{R,\sigma} \to \exp(i\theta)c_{R,\sigma}$ of the Hamiltonian, acquiring the best possible energy for a uniform superconducting phase. In this approach, Δ_{AF} turns out to be nonzero only at half filling but it is important to emphasize that, despite the uncorrelated HF case, a nonzero $d_{x^2-y^2}$ BCS pairing is possible at finite doping for T_{eff} lower than a critical effective temperature, and this represents one of the most important effect of electron correlation, as it is not present in the infinite T_{eff} HF theory.

In this way, we can determine the transition between the translationally invariant phase and the stripe phase as reported in Fig. 8 for the three representative values of U/t. Notice also that the location of the transition points does not depend much on the extrapolation, clearly supporting that the phase diagram converges quite fast by lowering T_{eff}.

As in HF theory, away from the commensurate dopings $1/W$, an insulating phase covering a continuum of different dopings can be constructed by appropriately joining such commensurate solutions, i.e., a doping $2/13$ with insulating properties can be easily obtained by alternating a $W = 7$ stripe with a $W = 6$ one. This is actually the case in a 26×12 cluster, within VAFQMC, namely, the $6 + 7 + 6 + 7$ alternating stripe length solution has an energy slightly lower than the corresponding one $6 + 6 + 7 + 7$, thus satisfying the HF rule stated at the end of the previous section. This phase, competing with the uniform $d_{x^2-y^2}$ BCS one, has a full charge gap in $H_{\text{MF}}(\boldsymbol{\alpha_0})$, a property that cannot be changed by a small τ projection. Moreover, no coexistence of stripe and BCS order was found within VAFQMC.

In summary, according to Fig. 8, it is possible to conclude that an insulating stripe phase acquires an energy lower than the corresponding uniform phase already at quite large doping, around $\delta \simeq 20\%$. Nevertheless, it is important to remark that the uniform phase has a very good energy, competing with the lowest possible ones. Indeed, in Fig. 4 the uniform d-wave phase loses only a tiny energy (less than $0.001t$ per site at the lowest T_{eff}) versus the nonuniform stripe phases. Interestingly, just around the doping $\delta = 1/8$ equally spaced stripes with length $W < 1/\delta$ appear lowest in energy, as can be seen in Fig. 9, where the energy of such metallic [at least within the mean-field Hamiltonian $H_{\text{MF}}(\boldsymbol{\alpha_0})$] stripes are compared with the commensurate insulating ones (black lines). For instance the $W = 9$ stripe at doping around $1/13$ (i.e., a metallic stripe with $W < 1/\delta$) has a hole energy more than $0.01t$ below the corresponding insulating stripe with $W = 13$, a huge gain that can be hardly explained by artifacts of the approximations (finite T_{eff} and/or finite clusters). In

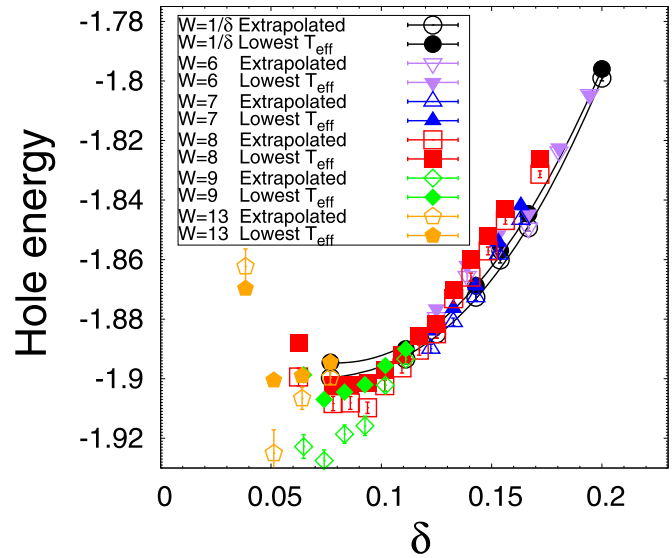

FIG. 9. Hole energy at $U/t = 8$ for equally spaced stripes of different lengths W as a function of the doping δ, by considering clusters of dimension larger than $12 \times 2W$, namely, enough to have negligible finite size effects. For doping around $\delta \simeq \frac{1}{8}$, stripes with length $W < \frac{1}{\delta}$ become energetically stable and acquire metallic character as the mean-field bands defining the variational wave function used in this paper are only partially filled. The commensurate stripe results with $\delta = 1/W$ are connected by black lines.

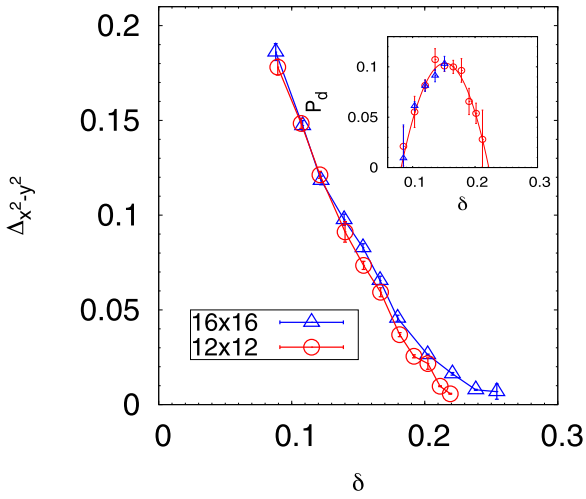

FIG. 10. $\Delta_{x^2-y^2}$ BCS pairing variational parameter in the mean-field Hamiltonian $H_{\rm MF}(\boldsymbol{\alpha_0})$ [see Eq. (21)] defining the spatially uniform variational ansatz of Eq. (2) as a function of the doping δ for the lowest $T_{\rm eff}$ and largest clusters considered. Inset: Value of the corresponding BCS order parameter evaluated with the $T_{\rm eff} \to 0$ linear extrapolation of the pairing-paring correlations at distance $L/2$. The error bars include also uncertainty in this extrapolation.

this plot, we also see that phase separation (a minimum of the hole energy) cannot be excluded for doping $\delta \lesssim 5\%$ but the results strongly depend on the extrapolation and therefore this would have to be settled by performing calculations at higher accuracy. By judging from the extrapolated values, it is plausible to expect a similar flat behavior of the energy per hole at low doping as in the corresponding HF plot [Fig. 7(a). However, within HF, a metallic solution with $W < 1/\delta$ was never found to have the lowest energy at low doping, again in agreement with Ref. [62].

In the remaining part of this section, we wish to extensively discuss the main result of this work, namely, that at large doping the stripe melts and a small but sizable superconducting d-wave order clearly remains within the present approach, in the sense that the energy is lowered in the thermodynamic limit by breaking the $U(1)$ global symmetry related to number of particle conservation. This is because both the mean-field Hamiltonians $H_{\rm MF}(\boldsymbol{\alpha_0})$ and $H_{\rm MF}(\boldsymbol{\alpha})$ clearly support a broken symmetry solution of this type when $\Delta_{x^2-y^2} > 0$ in Eq. (21). Indeed, in Fig. 10 the superconducting gap $\Delta_{x^2-y^2}$ parameter, corresponding to $H_{\rm MF}(\boldsymbol{\alpha_0})$, is displayed for $U/t = 8$ as a function of the doping. When the $\Delta_{x^2-y^2}$ is large, there are negligible size effects. However when it approaches zero, a long slowly decaying tail shows evident size effects. Indeed, with the largest affordable sizes it is possible that the calculated critical doping δ_c above which a symmetric phase is stable indicates only a sharp crossover region separating a phase with sizable strong coupling superconductivity from another phase with a very small order parameter, compatible with an exponentially small pairing of the Kohn-Luttinger type [28,66]. Indeed, within weak and intermediate couplings, the d-wave superconducting phase should remain stable up to $\simeq$40% doping, a doping much larger than the one detected in the present paper.

As shown in Fig. 11, within this approach, the critical doping characterizing a strong coupling superconductivity (i.e., a non-negligible pairing) can be identified because for $\mu \leqslant \mu_c$ the energy clearly improves by increasing the value of $\Delta_{x^2-y^2}$ even when starting from a negligible value, representing the symmetric Fermi liquid ground state. Nevertheless, there may be non-negligible size effects as shown for $U/t = 8$, especially considering the difficulty to locate the end of a long tiny tail of the order parameter, as discussed before. Moreover, for smaller U these size effects are expected to be even larger, but much larger cluster simulations are prohibitive at present. For this reason, for $U/t = 2$ ($U/t = 4$) a much larger mesh for the TABC was used with 64×64 (32×32) different twists in the BZ, instead of the smaller 16×16 grid used for $U/t = 8$ and $U/t = 6$. In a mean-field calculation, a 64×64 TABC grid in a 16×16 square lattice corresponds to a 1024×1024 cluster with PBC, large enough to probe even a very tiny but non-negligible gap parameter $\Delta_{x^2-y^2}$. Remarkably, at $U/t = 2$ no evidence of such a tiny value of the order parameter is found in all relevant doping region, as can be clearly seen in Fig. 11.

This small but relevant strong coupling region where d-wave superconductivity appears to be stable in the Hubbard model is in agreement with many different mean-field approaches [27,67–71], although its optimal doping is a matter of debate. Moreover, it is worth mentioning recent VMC calculations [72,73] and density matrix embedding theory [74] also supporting the stability of a $d-$wave superconductivity in a small doping region. On the other hand, the proposed phase diagram is also in agreement with the claim [29] of absence of $d-$wave superconductivity in the 2D Hubbard model, because in this paper the authors refer mainly to doping 1/8, where no BCS pairing was found also in this work. The final phase diagram is therefore reported in Fig. 12 [75].

VII. CONCLUSIONS

In this paper, the VAFQMC method, able to exploit the power of the auxiliary field technique combined with the simplicity and generality of the standard variational quantum Monte Carlo method, has been introduced. By combining these two successful approaches to strongly correlated systems, it is possible to estimate the evolution of the phase diagram of a lattice model by improving systematically the accuracy of the correlation term, starting from the HF approximation. This is achieved by lowering an effective temperature $T_{\rm eff}$ up to a value that turns out to be low enough to provide very accurate variational energies of the Hubbard model in the thermodynamic limit, while remaining far from any sign problem instability, so far affecting most fermion quantum Monte Carlo techniques. Within the assumption that the tiny energy gain between different broken-symmetry phases of the model can be sorted out by a careful optimization of a mean-field ansatz in the presence of an accurate enough correlation term, the phase diagrams obtained in this way should be considered reliable, at least for the phases studied.

It is clear that the above assumption is very important as, for instance, in the Hubbard model, we have estimated an energy per site error of about $2 \times 10^{-3}t$ ($4 \times 10^{-4}t$) at $U/t = 8$ ($U/t = 4$), while energy differences of the various

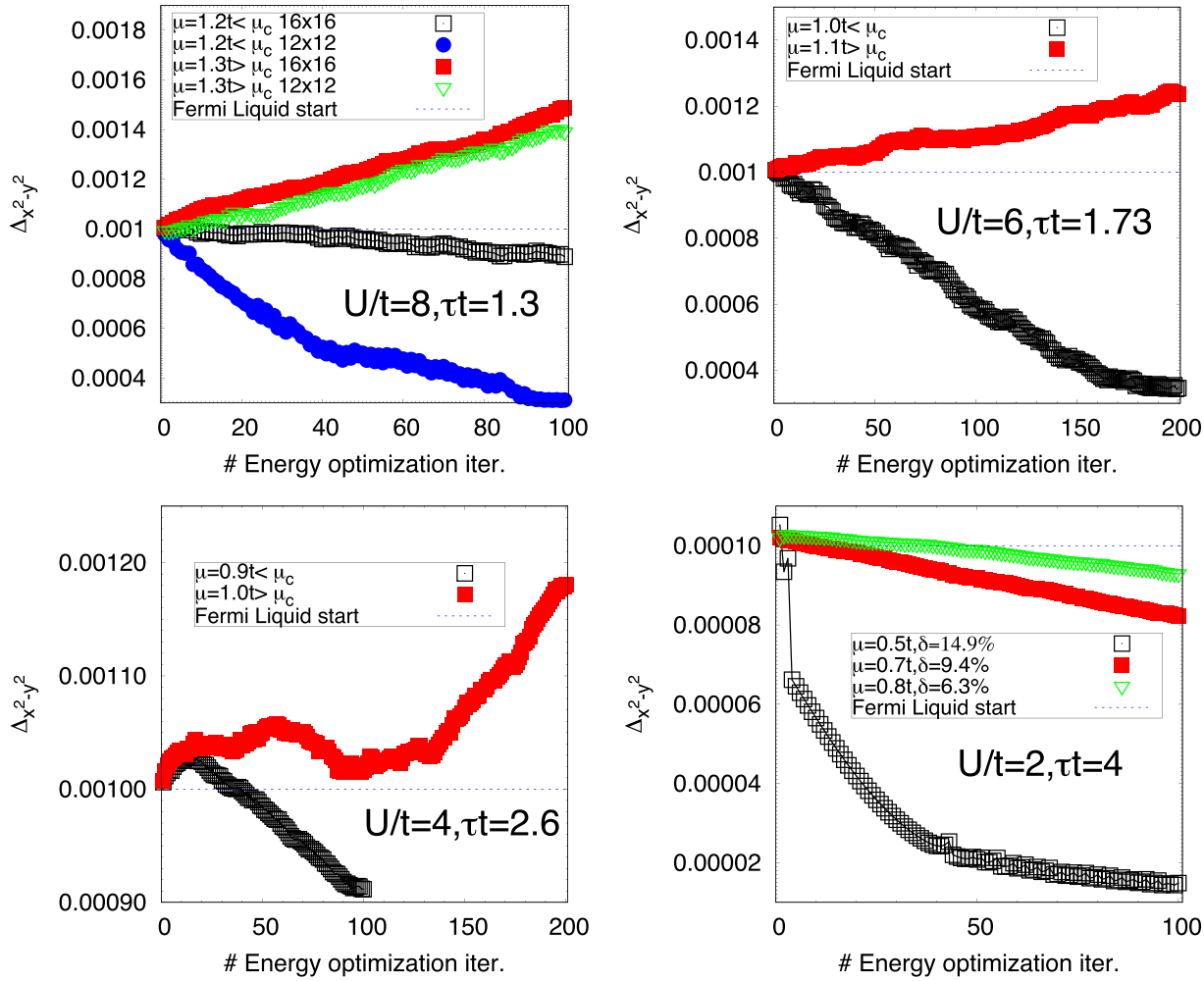

FIG. 11. $\Delta_{x^2-y^2}$ BCS pairing variational parameter in the mean-field Hamiltonian $H_{\rm MF}(\boldsymbol{\alpha_0})$ defining the spatially uniform variational ansatz of Eq. (2) as a function of the energy optimization iterations at the lowest $T_{\rm eff}$ (i.e., largest $\tau t = 4, 2.6, 1.73, 1.3$ for $U/t = 2, 4, 6, 8$, respectively) and 16×16 cluster. For all cases, the initial wave function was prepared with $\Delta_{x^2-y^2} = 0$ defining the Fermi liquid state. Then this parameter was set to a small value and the iterative stochastic optimization was started. In these calculations, to reduce at most the stochastic bias, at each iteration a quite large number ($>3 \times 10^5$) of samples for evaluating energy derivatives was used, in a way that they are sensitive to very small energy differences $<10^{-5}t$. Optimization of the grand potential Ω at fixed chemical potential μ was employed in all cases shown. The corresponding doping was estimated by $\frac{\partial \Omega}{\partial \mu} = -(1-\delta)N_s$ using the data for Ω reported in the Supplemental Material extrapolated to the $T_{\rm eff} \to 0$ limit. These estimates are consistent with the direct evaluation of the doping $\delta = 1 - \frac{\langle \psi_\tau | \hat{N} | \psi_\tau \rangle}{N_s \langle \psi_\tau | \psi_\tau \rangle}$ at the lowest $T_{\rm eff}$ within half the confidence doping interval reported for each $U/t \neq 2$.

phases at the lowest $T_{\rm eff}$ considered can be even more than an order of magnitude smaller. This is not a difficulty of the present method, providing state-of-the-art variational energies (see Supplemental Material for detailed benchmark results), but clarifies once more the enormous challenge of the electron correlation problem in numerical calculations. For instance, on such clusters it is basically impossible to distinguish an unbroken symmetric metallic phase from a d-wave superconducting one with a small $\Delta_{x^2-y^2}$ gap parameter, by judging merely on correlation functions (e.g., pairing correlations), and the above assumption provides a much more sensitive criterium for occurrence of broken symmetry phenomena. Relying on the above assumption dramatically helps numerical techniques, such as VAFQMC, able to work with boundary conditions fulfilling the symmetries of H, that may be possibly broken in the thermodynamic limit.

In any case, the present paper provides rigorous and accurate upper bounds of the ground-state energies of the Hubbard model for several U/t and doping values well converged in the thermodynamic limit (see Supplemental Material) that can be useful in future works on this important subject and/or for benchmarking computational, theoretical or experimental techniques. The fact that extrapolated energies do not depend much on the ansatz adopted (all extrapolated energies agree within $0.001t$ per site) implies that energetic properties are settled within a reasonable accuracy. However, to get the right order without assuming it in the initial mean-field ansatz, much larger projection times are required (see, for instance, Fig. 4 where two completely different phases differ in energy by less than $0.001t$ per site), that are at present not possible.

In this paper, many different mean-field solutions have been attempted with several different initializations of

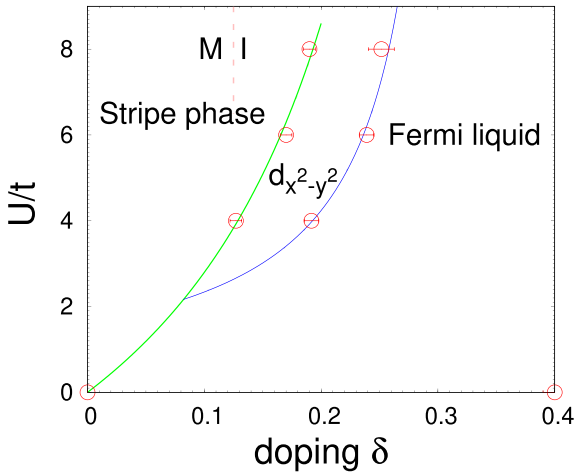

FIG. 12. Phase diagram of the Hubbard model by VAFQMC. Blue and green continuous lines are simple interpolations of the transition points (open circles, $\delta = 19\% - 25.2\%, 17\% - 23.9\%, 12.7\% - 18.6\%$ for $U/t = 8, 6, 4$, respectively). The blue line is also determined by the condition that for $U/t = 2$ no BCS pairing has been detected, while the green line by the one that the incommensurate spin order cannot show up at nonzero doping for $U \to 0$ [62]. In the stripe phase, there may be a transition between an insulating stripe and a small doping metallic stripe, as suggested by Fig. 9 for $U/t = 8$. In this transition, the mean-field VAFQMC Hamiltonian $H_{\rm MF}(\boldsymbol{\alpha_0})$ has a finite gap (bands are completely filled) or a vanishing one, respectively.

parameters, also including broken time-reversal solutions [76] and different modulations of stripes and pairing. In all cases, the smooth convergence of the energy as a function of $T_{\rm eff}$ has been verified. This is not only important for achieving reasonable extrapolations but especially for excluding being trapped in spurious local minima, which is a limitation of any nonlinear optimization technique. The phase diagram presented here in Fig. 12 shows the phases so far determined with the lowest possible variational energies among the chosen ansatzs.

Hereupon, a remark is needed: a systematic analysis of the convergence toward the ground state for different choices of the trial WFs and projector operator's ansatz (e.g., using d_{xy} instead of $d_{x^2-y^2}$ symmetries) is still required. However, it is beyond the scope of this paper, since it may require a precise analysis of different models, being one of our outlooks.

An important progress in this paper is the control of finite-size effects within VAFQMC. The conventional approach is to attempt exact calculations (usually very hard if not impossible) at finite number of sites N_s and try to extrapolate to $\frac{1}{N_s} \to 0$. Within VAFQMC, it is much simpler and indeed possible to extrapolate only in the effective temperature $T_{\rm eff} \to 0$ limit the finite $T_{\rm eff} \gtrsim t/2$ results. To this purpose, it is enough to perform $N_s \gtrsim 100$ calculations because they are already very close to the $\frac{1}{N_s} \to 0$ limit, thanks to the very effective twisted average boundary condition method.

The results shown in this paper are weakly affected by the sign problem. In general, the average sign, appearing, for instance, in the denominator of Eq. (16), should decay exponentially to zero both with $1/T_{\rm eff}$ and N_s, yielding prohibitive statistical errors. However, for $T_{\rm eff}$ large enough (i.e., the ones used here), the exponential decay in N_s of the average sign is very weak due to a stability property of the adopted auxiliary field technique that was discovered several years ago [77]. Hence, much larger clusters could be safely simulated, a very promising possibility if one considers that the ones reported here are not far from state-of-the-art simulations not vexed by the sign problem.

In this paper, a large stripe phase in the Hubbard model exists as an effective way to expel the holes from a clean antiferromagnet. In this way, genuine phase separation does not occur in the Hubbard model as a result of a very weak repulsive coupling between stripes at large distances. In practice, at small doping, the energy per hole is almost constant, namely, the inverse charge compressibility is vanishingly small, in agreement with the phase separation scenario [64] and some previous numerical calculations [78–80].

An important outcome of the present paper is that a sizable superconducting phase is present in the Hubbard model with a non-negligible order parameter only in the strong coupling regime. For instance, for $U/t = 2$ no evidence of $d_{x^2-y^2}$ BCS order was probed and the maximum $\Delta_{x^2-y^2} \simeq 0.02t$ was obtained with the largest $U/t = 8$ considered at about 20% doping. The critical doping δ_c separating the metal from the d-wave superconductor turns out to be much smaller than the one obtained for weak and intermediate coupling analysis [28,66], and the question is how to reconcile the weak and the strong coupling limits. In principle, as suggested by the results in Fig. 10, a small tail with very weak BCS pairing could distinguish a strong coupling phase with sizable pairing and a weak coupling phase with a sharp crossover (and not a transition) clearly separating the two regimes.

The main features of cuprate superconductivity can be explained with the Hubbard model, but quantitatively there remain several unsolved issues. First, the stripes are completely filled by holes and do not match the half filled ones detected experimentally [81]. Second, the d-wave superconductivity is sizable but still far from explaining $T_c \simeq 100\,{\rm K}$ because the gap function that is growing when approaching the Mott insulating phase at zero doping (see Fig. 10) is limited by the phase transition to the stripe phase.

VAFQMC has been developed to study properties of strongly correlated systems in the thermodynamic limit. Obviously, this method applies also to finite systems for obtaining the best ground-state estimates with the largest possible projection time τ. However, for finite systems, the symmetry is never broken, and a more accurate WF should be used by restoring the symmetry with appropriate projection operators [82,83], an improvement that can be done and should be worth doing for this particular purpose. Moreover, several applications and extensions are possible within VAFQMC. The WF $|\psi_\tau\rangle$ can be further generalized to more realistic Hamiltonians, including, for instance, long-range Coulomb interaction or electron-phonon coupling. The finite effective temperature $T_{\rm eff}$ here defined for a variational WF is the key to obtaining very accurate results well converged in the thermodynamic limit, a feature that could be possibly generalized to several other computational techniques, from tensor networks to machine-learning variational WFs.

ACKNOWLEDGMENTS

I am particularly in debt to A. Parola, N. Costa, and E. Tosatti for several suggestions for improving the paper. I am also grateful for very useful discussions with G. Carleo, N. Costa, A. Tirelli, F. Becca, L. Capriotti, and M. Fabrizio. I acknowledge PRACE for awarding access to Marconi at CINECA Italy, and Riken collaboration for access to HOKUSAI supercomputer in Saitama Japan, as well as financial support from the MIUR Progetti di Ricerca di Rilevante Interesse Nazionale (PRIN) Bando 2017, Grant No. 2017BZPKSZ and the Simons Foundation. This work is supported by the European Centre of Excellence in Exascale Computing TREX - Targeting Real Chemical Accuracy at the Exascale. This project has received funding from the European Union's Horizon 2020 Research and Innovation program under Grant Agreement No. 952165. Finally, I thank Natanael Costa and Andrea Tirelli for revising the latest version of this paper.

APPENDIX A: FINITE EFFECTIVE TEMPERATURE T_{eff} CORRECTIONS FOR THE INFINITE VOLUME GROUND STATE PROJECTION

Given a $\tau/2$-projected trial function $|\psi_\tau\rangle = \exp(-H\tau/2)|\psi_{\text{MF}}\rangle$, the pseudopartition function,

$$Z(\tau) = \langle\psi_\tau|\psi_\tau\rangle = \langle\psi_{\text{MF}}|\exp(-\tau H)|\psi_{\text{MF}}\rangle, \tag{A1}$$

is considered in the following, namely, with an effective temperature $T_{\text{eff}} = \frac{1}{\tau}$ fixed when the infinite volume thermodynamic limit is employed. Here the particular case of the Heisenberg model $H = J\sum_{<ij>}\vec{S}_i\cdot\vec{S}_j$ and $|\psi_{\text{MF}}\rangle = |\text{Néel}\rangle$ is studied, but, due to universality, the results should apply to any model, where a classical symmetry, parametrized by an $M-$dimensional real vector is broken. In particular, it holds for the WF of Eq. (1) in the main text for collinear magnetic order $M = 3$ (applies also for the stripe phase) and the superconducting $M = 2$ one. In the Heisenberg model, in D dimensions, the low-energy limit can be studied by introducing coherent states $\vec{n}$ with $|\vec{n}|^2 = 1$ and, by integrating over one of the two sublattices [84], it follows that

$$Z = \int d[\vec{n}]_{0,\tau}\exp \times\left\{-\frac{1}{2}\int_0^\tau dt\int dr^D\left[\chi|\partial_t\vec{n}|^2 + \Upsilon\sum_{\nu=1}^{D}|\partial_\nu\vec{n}|^2\right]\right\} \tag{A2}$$

with the notations given in Ref. [44], where Υ is the spin-wave stiffness and χ is the transverse susceptibility. In the case of the pseudopartition function of Eq. (A2), the following boundary conditions for the $M-$ component field $\vec{n}(\vec{r},t)$ hold:

$$\vec{n}(\vec{r},0) = \vec{n}(\vec{r},\tau) = (1,0,\cdots,0), \tag{A3}$$

because the field at the boundary of the time interval is constrained to have the value of the trial function $|\psi_{\text{MF}}\rangle$, a Néel state with the antiferromagnetic order along the x axis.

Due to the above boundary conditions, the $M-1$ component vector $\vec{\Pi}$, describing the field fluctuations, and defined by

$$\vec{n}(\vec{r},t) = (1-\frac{|\vec{\Pi}(\vec{r},t)|^2}{2},\vec{\Pi}(\vec{r},t)) + o(\Pi^2) \tag{A4}$$

acquires the following Fourier decomposition:

$$\vec{\Pi}(\vec{r},t) = \sqrt{\frac{2}{\tau V}}\sum_{n>0,\vec{q}}\vec{\Pi}_{n,\vec{q}}\sin(\omega_n t)\exp(i\vec{q}\cdot\vec{r}), \tag{A5}$$

where $\vec{q} = \frac{2\pi}{L}(n_x,n_y,\cdots)$ are the momenta allowed by the PBCs, whereas $\omega_n = \frac{\pi n}{\tau}$ for integers $n > 0$ to satisfy that the field vanishes at $t = 0$ and $t = \tau$. Notice that, in the usual partition function at finite temperature $T = \frac{1}{\tau}$, the quantization of the frequencies $\omega_n = \frac{2\pi n}{\tau}$ (also nonpositive integers allowed) is slightly different and the calculations can be easily generalized, but they have already been reported in previous works [44–46]. Therefore, we just mention in the following the standard finite temperature case to check the results derived in this section.

With the above definition, the pseudopartition function acquires a Gaussian form at leading order, valid in the ordered phase:

$$Z = \int[d\vec{\Pi}]\exp\left\{-\frac{1}{2}\sum_{n,\vec{q}}\left(\chi\omega_n^2+\Upsilon|\vec{q}|^2\right)|\vec{\Pi}_{n,\vec{q}}|^2\right\} \propto \exp\left\{-\frac{M-1}{2}\sum_{n,\vec{q}}\ln\left(\chi\omega_n^2+\Upsilon|\vec{q}|^2\right)\right\}. \tag{A6}$$

On the other hand, the average propagator over these Gaussian fluctuations can be readily evaluated,

$$\left\langle\Pi^\nu_{n,\vec{q}}\Pi^\nu_{n,-\vec{q}}\right\rangle = \frac{1}{\chi\omega_n^2+\Upsilon|\vec{q}|^2}, \tag{A7}$$

where $\nu = 1,2,\cdots M-1$ labels the components of the vector $\vec{\Pi}$.

1. Energy and order parameter

The expectation value of the energy $E(\tau)$ over the state $|\psi_\tau\rangle = \exp(-H\tau/2)|\psi_{\text{MF}}\rangle$ can be written as

$$E(\tau) = -\partial_\tau\ln Z. \tag{A8}$$

Since $E(\tau)$ in the expression Eq. (A6) depends on τ only by means of ω_n, it follows that

$$E(\tau) = -\frac{(M-1)}{\tau}\sum_{n>0,\vec{q}}\frac{\chi\omega_n^2}{\chi\omega_n^2+\Upsilon|\vec{q}|^2}. \tag{A9}$$

On the other hand, the local magnetization,

$$m(\tau) = \frac{\langle\psi_\tau|\frac{1}{V}\int d\vec{r}^D\left(1-\frac{\Pi(\vec{r},\tau/2)^2}{2}\right)|\psi_\tau\rangle}{\langle\psi_\tau|\psi_\tau\rangle}, \tag{A10}$$

can be easily evaluated by the knowledge of the propagator in Eq. (A7) and the definition of the component in the ordered x direction in Eq. (A4):

$$m(\tau) = 1-\frac{(M-1)}{V\tau}\sum_{n>0,\vec{q}}\frac{\sin(\frac{\omega_n\tau}{2})^2}{\chi\omega_n^2+\Upsilon|\vec{q}|^2}. \tag{A11}$$

2. Evaluation

As in any field theory, the above expressions diverge without introducing infinite counter terms. In the expression of the energy, one can subtract and add one in the integrand, whereas in the correction of the magnetic moment it is enough to deal with particular care the $q = 0$ mode (this mode may also be avoided by using twisted boundary conditions):

$$E/V = \frac{M-1}{\tau V}\sum_{n>0,\vec{q}}\frac{\Upsilon|\vec{q}|^2}{\chi\omega_n^2+\Upsilon|\vec{q}|^2} - \frac{M-1}{\tau V}\sum_{n>0,\vec{q}}1,$$

$$m(\tau) = 1 - \frac{(M-1)}{V\tau}\sum_{n>0,\vec{q}}\frac{\sin\left(\frac{\omega_n\tau}{2}\right)^2}{\chi\omega_n^2+\Upsilon|\vec{q}|^2}. \tag{A12}$$

The infinite right-hand side term in the energy corresponds to an infinite shift of the ground-state energy, a typical feature of quantum field theories, as this shift becomes finite by introducing a cutoff, implicitly present in any physical model.

To evaluate the above expressions, it is useful to consider the following sum:

$$\sum_n \frac{1}{z+n} = \pi\cot(\pi z), \tag{A13}$$

which is valid for any complex number z. In particular, for $z = \frac{1}{2} + iy$ we obtain

$$\sum_n \frac{1}{\frac{1}{2}+iy+n} = -i\pi\tanh(\pi y), \tag{A14}$$

whereas for $z = iy$ we get

$$\sum_n \frac{1}{iy+n} = -i\pi\coth(\pi y). \tag{A15}$$

Defining the velocity of the Goldstone's modes $c = \sqrt{\frac{\Upsilon}{\chi}}$, the sum over n is extended to $-\infty \leqslant n \leqslant \infty$, using the even dependence on n and taking into account the extra $n = 0$ contribution in the definition of ϵ_0. In this way, by using Eq. (A15) for evaluating the infinite sums, the universal finite size corrections are given by

$$\begin{aligned} E/V &= \frac{M-1}{2\tau V}\sum_{n=-\infty}^{\infty}\sum_{\vec{q}}\frac{i\sqrt{\Upsilon}|q|}{2}\left[\frac{1}{\sqrt{\chi}\omega_n + i\sqrt{\Upsilon}|q|}\right. \\ &\quad \left. - \frac{1}{\sqrt{\chi}\omega_n - i\sqrt{\Upsilon}|q|}\right] - \frac{M-1}{2\tau V}\sum_{n=-\infty}^{\infty}\sum_{\vec{q}}1 \\ &= \epsilon_0 + \frac{(M-1)c}{2V}\sum_{\vec{q}}|q|(\coth(c|q|\tau)-1), \end{aligned} \tag{A16}$$

where ϵ_0 is the "infinite" ground-state energy corrected for the zero-point harmonic energy $\epsilon_0 = \frac{M-1}{2V}\sum_{\vec{q}} c|q| - \frac{M-1}{\tau 2V}\sum_{n=-\infty}^{\infty}\sum_{\vec{q}}1$, a divergent expression depending on the cutoff but not on the boundary conditions (i.e., it is the same divergent term appearing in Ref. [44] by using the trace). In the thermodynamic limit and fixed τ, the convergent contribution can be worked out by replacing sums over momenta with integrals (i.e., $\frac{1}{V}\sum_q \to \int(\frac{dq}{2\pi})^D$), and changing the momentum scale $\vec{q} \to c\tau\vec{q}$, so that

$$E/V = \epsilon_0 + \frac{(M-1)}{2c^D}f_e T_{\rm eff}^{D+1}, \tag{A17}$$

where f_e is a dimensional dependent constant defined by

$$f_e = \int\left(\frac{dq}{2\pi}\right)^D |q|(\coth(|q|)-1), \tag{A18}$$

which is clearly a convergent integral for any dimension $D \geqslant 1$ because $\coth(|q|)$ converges to one exponentially for large $|q|$. The values of f_e are therefore $\frac{\pi}{12}$, $\frac{\zeta(3)}{4\pi}$ ($\zeta(3) = 1.20205690316$) and $\frac{\pi^2}{240}$ in $D = 1$, $D = 2$ and $D = 3$, respectively. In $D = 1$, the coefficient f_e is not to be taken for granted, since no true long-range order is possible (see later), but the qualitative behavior of the correction $\simeq T_{\rm eff}^2$ should hold as it is consistent with the corresponding finite temperature correction derived in $D = 1$ for the 1D-Hubbard model by means of the Bethe ansatz [85].

Thus, in the thermodynamic limit, the finite τ corrections to the energy depend only on the universal constant f_e, the number of components M of the order parameter, and the velocity c of the gapless Goldstone modes. In $D = 2$, the finite temperature corrections to the internal energy at infinite volume have been determined in Ref. [45]. For this purpose, we have repeated the same type of calculation and get that, taking into account the different boundary conditions for the field (PBC in time for the trace $\tau = \beta = 1/T$),

$$\begin{aligned} E(T)/V - \epsilon_0 &= \frac{(M-1)c}{2}\int\left(\frac{dq}{2\pi}\right)^D |q| \\ &\quad \times\left(\coth\left(\frac{c|q|\beta}{2}\right)-1\right) \\ &= \frac{(M-1)c}{2\left(\frac{c}{2T}\right)^{D+1}}f_e, \end{aligned} \tag{A19}$$

which is consistent with the previous calculation reported in $D = 2$, i.e., [45]:

$$E(T)/V - \epsilon_0 = (M-1)\frac{\zeta(3)}{c^2\pi}T^3. \tag{A20}$$

On the other hand, for the magnetic order parameter, by noticing that $\sin(\frac{\omega_n\tau}{2})^2 = 1$ for $n = 2\nu+1$ and zero otherwise, the sum has to be evaluated for odd integer frequencies $\omega_\nu = \frac{\pi(2\nu+1)}{\tau}$. For this purpose, the sum $\sum_{\nu=0}^{\infty}\frac{1}{\chi\omega_\nu^2+\Upsilon|\vec{q}|^2}$ is extended to $\frac{1}{2}\sum_{\nu=-\infty}^{\infty}\frac{1}{\chi\omega_\nu^2+\Upsilon|\vec{q}|^2}$ because $\omega_\nu = -\omega_{-(\nu+1)}$ for $\nu < 0$. Therefore, by applying Eq. (A14) for evaluating the following infinite sums, one obtains

$$\begin{aligned} \Delta m(\tau) &= -\frac{M-1}{2V\tau}\sum_{\nu,\vec{q}}\frac{i}{2\sqrt{\Upsilon}|q|}\left[\frac{1}{\frac{\sqrt{\chi}\pi}{\tau}(2\nu+1)+i\sqrt{\Upsilon}|q|}\right. \\ &\quad \left. - \frac{1}{\frac{\sqrt{\chi}\pi}{\tau}(2\nu+1)-i\sqrt{\Upsilon}|q|}\right] \\ &= -\frac{M-1}{4V\sqrt{\chi\Upsilon}}\sum_{\vec{q}\neq 0}\frac{(\tanh(c|q|\tau/2)-1)}{|q|} - \Delta m_0 \\ &= -\Delta m_0 - \frac{M-1}{4\sqrt{\chi\Upsilon}c^{D-1}}f_m T_{\rm eff}^{D-1}, \end{aligned} \tag{A21}$$

where $\Delta m_0 = \frac{(M-1)\tau}{8V\chi} + \frac{M-1}{4\sqrt{\chi\Upsilon V}}\sum_{\vec{q}\neq 0}\frac{1}{|q|}$ [the first term in Δm_0 is the $q=0$ contribution in Eq. (A12) that is convergent for finite τ] and the dimensional dependent constant f_m is defined by

$$f_m = \int \left(\frac{dq}{2\pi}\right)^D \left(\tanh\left(\frac{|q|}{2}\right) - 1\right) \Big/ |q|, \tag{A22}$$

which converges in $D > 1$. The values of f_m are therefore $-\frac{\ln(2)}{\pi}$ and $-\frac{1}{12}$ for $D = 2$ and $D = 3$, respectively.

Thus, in the thermodynamic limit the finite T_{eff} corrections to the antiferromagnetic order parameter depend on the universal constant f_m, the number of components M of the order parameter, the velocity c, and the stiffness Υ of the gapless Goldstone modes.

Notice that the expression above for f_m converges in $D = 2$. Instead, if PBCs in τ are assumed for the field $\vec{\Pi}(x,t)$, corresponding to the standard finite temperature calculation at $\beta = \tau$, by repeating the same steps, it follows that $\Delta m(\tau) = -\frac{M-1}{2V\sqrt{\chi\Upsilon}}\sum_{q\neq 0}\frac{\coth(c|q|\tau/2)}{|q|}$, which blows up for $D \leqslant 2$, thus recovering the Mermin-Wagner theorem [86]: no finite m is possible at finite temperature for $D \leqslant 2$. The advantage of using the projection technique is therefore evident especially in $D = 2$ for the study of broken symmetry phases that are possible, for continuous symmetries, only at zero temperature.

When using finite cylinders with even L_y, all the above results obtained for $D = 1$ apply because the y momentum $q_y = \frac{2\pi n_y}{L_y}$ is quantized with $n_y = 0, 1, \cdots, L_y - 1$ and only the $q_y = 0$ momentum value provides power law corrections in $1/\tau$ to energy and correlation functions (if converging). This is because all the other contributions acquire a finite $\sim\frac{1}{L_y}$ gap and converge much faster.

APPENDIX B: CONVEXITY OF THE ENERGY AS A FUNCTION DENSITY

One can divide a large system $A + B$ in two regions A and B containing a macroscopic number of sites L_A and L_B and electrons N_A and N_B, respectively. Then, by defining E_{A+B} the energy of the total system, E_A and E_B the ones of the corresponding parts, $\rho = \frac{N_A+N_B}{L_A+L_B} = p\rho_1 + (1-p)\rho_2$, $\rho_1 = \frac{N_A}{L_A}$, $\rho_2 = \frac{N_B}{L_B}$, $p = \frac{L_A}{L_A+L_B}$, $e(\rho_1) = E_A/L_A$, and $e(\rho_2) = E_B/L_B$ converged in the thermodynamic limit because the two parts are macroscopic, then $e(\rho) = \frac{E_{A+B}}{L_A+L_B} \leqslant \frac{E_A+E_B}{L_A+L_B} = pe(\rho_1) + (1-p)e(\rho_2)$ follows because one can neglect in the thermodynamic limit the surface term contribution to the energy separating region A from region B. This is because, by assumption, the model is short range as the hopping term connects only nearest-neighbor sites and the interaction U is on site. The final inequality,

$$e(\rho) \leqslant pe(\rho_1) + (1-p)e(\rho_2), \tag{B1}$$

therefore holds for arbitrary densities $\rho_1 \leqslant \rho \leqslant \rho_2$ and implies the convexity property of the function $e(\rho)$ in the thermodynamic limit. Whenever phase separation occurs between two densities ρ_1 and ρ_2, the inequality (B1) turns to a strict equality, namely, $e(\rho)$ is a linear function of the density because $p = \frac{\rho-\rho_2}{\rho_1-\rho_2}$, so, in particular, the energy per hole in Eq. (20) is constant for $\delta \leqslant \delta_c$.

[1] W. Kohn and L. J. Sham, Phys. Rev. **140**, A1133 (1965).
[2] S. R. White, Phys. Rev. Lett. **69**, 2863 (1992).
[3] U. Schollwöck, Rev. Mod. Phys. **77**, 259 (2005).
[4] R. Orús, Ann. Phys. **349**, 117 (2014).
[5] F. Verstraete, D. Porras, and J. I. Cirac, Phys. Rev. Lett. **93**, 227205 (2004).
[6] N. Schuch, D. Pérez-García, and I. Cirac, Phys. Rev. B **84**, 165139 (2011).
[7] R. Blankenbecler, D. J. Scalapino, and R. L. Sugar, Phys. Rev. D **24**, 2278 (1981).
[8] J. E. Hirsch, Phys. Rev. B **31**, 4403 (1985).
[9] S. R. White, D. J. Scalapino, R. L. Sugar, E. Y. Loh, J. E. Gubernatis, and R. T. Scalettar, Phys. Rev. B **40**, 506 (1989).
[10] S. Sorella, S. Baroni, R. Car, and M. Parrinello, Europhys. Lett. **8**, 663 (1989).
[11] S. Zhang, J. Carlson, and J. E. Gubernatis, Phys. Rev. B **55**, 7464 (1997).
[12] A. W. Sandvik, Phys. Rev. B **59**, R14157 (1999).
[13] G. H. Booth, A. Grüneis, G. Kresse, and A. Alavi, Nature (London) **493**, 365 (2013).
[14] W. Dobrautz, H. Luo, and A. Alavi, Phys. Rev. B **99**, 075119 (2019).
[15] Y. Yao, E. Giner, J. Li, J. Toulouse, and C. J. Umrigar, J. Chem. Phys. **153**, 124117 (2020).
[16] G. Carleo and M. Troyer, Science **355**, 602 (2017).
[17] G. Carleo, I. Cirac, K. Cranmer, L. Daudet, M. Schuld, N. Tishby, L. Vogt-Maranto, and L. Zdeborová, Rev. Mod. Phys. **91**, 045002 (2019).
[18] E. H. Lieb and F. Y. Wu, Phys. Rev. Lett. **20**, 1445 (1968).
[19] A. Kitaev, Ann. Phys. **321**, 2 (2006), January Special Issue.
[20] A. Mazurenko, C. S. Chiu, G. Ji, M. F. Parsons, M. Kanász-Nagy, R. Schmidt, F. Grusdt, E. Demler, D. Greif, and M. Greiner, Nature (London) **545**, 462 (2017).
[21] D. P. Arovas, E. Berg, S. A. Kivelson, and S. Raghu, Annu. Rev. Condens. Matter Phys. **13**, 239 (2022).
[22] M. Qin, T. Schäfer, S. Andergassen, P. Corboz, and E. Gull, Annu. Rev. Condens. Matter Phys. **13**, 275 (2022).
[23] K. Seki and S. Sorella, Phys. Rev. B **99**, 144407 (2019).
[24] J. P. F. LeBlanc, A. E. Antipov, F. Becca, I. W. Bulik, G. K.-L. Chan, C.-M. Chung, Y. Deng, M. Ferrero, T. M. Henderson, C. A. Jiménez-Hoyos, E. Kozik, X.-W. Liu, A. J. Millis, N. V. Prokof'ev, M. Qin, G. E. Scuseria, H. Shi, B. V. Svistunov, L. F. Tocchio, I. S. Tupitsyn, S. R. White, S. Zhang, B.-X. Zheng, Z. Zhu, and E. Gull (Simons Collaboration on the Many-Electron Problem), Phys. Rev. X **5**, 041041 (2015).
[25] B.-X. Zheng, C.-M. Chung, P. Corboz, G. Ehlers, M.-P. Qin, R. M. Noack, H. Shi, S. R. White, S. Zhang, and G. K.-L. Chan, Science **358**, 1155 (2017).

[26] S. Zhang, J. Carlson, and J. E. Gubernatis, Phys. Rev. Lett. **78**, 4486 (1997).

[27] T. A. Maier, M. Jarrell, T. C. Schulthess, P. R. C. Kent, and J. B. White, Phys. Rev. Lett. **95**, 237001 (2005).

[28] Y. Deng, E. Kozik, N. V. Prokofev, and B. V. Svistunov, Europhys. Lett. **110**, 57001 (2015).

[29] M. Qin, C.-M. Chung, H. Shi, E. Vitali, C. Hubig, U. Schollwöck, S. R. White, and S. Zhang (Simons Collaboration on the Many-Electron Problem), Phys. Rev. X **10**, 031016 (2020).

[30] S. Sorella, G. B. Martins, F. Becca, C. Gazza, L. Capriotti, A. Parola, and E. Dagotto, Phys. Rev. Lett. **88**, 117002 (2002).

[31] The VMC relies on the variational principle: The best wave function ansatz, defined by a set of variational parameters, is the one that minimizes the expectation value of the Hamiltonian studied.

[32] P. Corboz, T. M. Rice, and M. Troyer, Phys. Rev. Lett. **113**, 046402 (2014).

[33] Considering the same unit, the order parameter was consistent with the previous calculation obtained by VMC [30] at around 15% doping.

[34] F. Becca and S. Sorella, *Quantum Monte Carlo Approaches for Correlated Systems* (Cambridge University Press, Cambridge, England, 2017).

[35] C. J. Umrigar, J. Toulouse, C. Filippi, S. Sorella, and R. G. Hennig, Phys. Rev. Lett. **98**, 110201 (2007).

[36] E. Y. Loh, J. E. Gubernatis, R. T. Scalettar, S. R. White, D. J. Scalapino, and R. L. Sugar, Phys. Rev. B **41**, 9301 (1990).

[37] D. Eichenberger and D. Baeriswyl, Phys. Rev. B **76**, 180504(R) (2007).

[38] T. Yanagisawa, S. Koike, and K. Yamaji, J. Phys. Soc. Jpn. **67**, 3867 (1998).

[39] T. Yanagisawa, J. Phys. Soc. Jpn. **85**, 114707 (2016).

[40] M. J. S. Beach, R. G. Melko, T. Grover, and T. H. Hsieh, Phys. Rev. B **100**, 094434 (2019).

[41] D. Wecker, M. B. Hastings, and M. Troyer, Phys. Rev. A **92**, 042303 (2015).

[42] S. Sorella, Phys. Rev. Lett. **80**, 4558 (1998).

[43] S. Amari, Neural Comput. **10**, 251 (1998).

[44] D. S. Fisher, Phys. Rev. B **39**, 11783 (1989).

[45] P. Hasenfratz and F. Niedermayer, Z. Phys. B **92**, 91 (1993).

[46] C. P. Hofmann, Phys. Rev. B **81**, 014416 (2010).

[47] C. Lin, F. H. Zong, and D. M. Ceperley, Phys. Rev. E **64**, 016702 (2001).

[48] C. Gros, Phys. Rev. B **53**, 6865 (1996).

[49] S. Karakuzu, K. Seki, and S. Sorella, Phys. Rev. B **98**, 075156 (2018).

[50] From this point of view, VAFQMC is not different from standard AFQMC or VMC and the expectation value of any operator, not only H, can be computed without particular effort [34].

[51] The numerator and the denominator of Eq. (14) are both real after summations over σ and σ' because they correspond to the RHS of Eq. (11) and the Hamiltonian is Hermitian. Therefore, the real part Re can be moved inside the summations of Eq. (14) with no approximation.

[52] A. Griewank, *Evaluating Derivatives: Principles and Techniques of Algorithmic Differentiation* (Frontiers in Applied Mathematics, Philadelphia, 2000).

[53] A. Griewank, Documenta Math. **Extra Volume**, 389 (2012).

[54] S. Sorella and L. Capriotti, J. Chem. Phys. **133**, 234111 (2010).

[55] H.-J. Liao, J.-G. Liu, L. Wang, and T. Xiang, Phys. Rev. X **9**, 031041 (2019).

[56] Convergence in the thermodynamic limit has also been verified by comparing with the 4×32 cluster within an error of about $0.0001t$.

[57] See Supplemental Material at http://link.aps.org/supplemental/10.1103/PhysRevB.107.115133 for more details about (i) uniform, and (ii) stripe wave function parametrizations.

[58] L. F. Tocchio, A. Montorsi, and F. Becca, SciPost Phys. **7**, 021 (2019).

[59] P. Corboz, P. Czarnik, G. Kapteijns, and L. Tagliacozzo, Phys. Rev. X **8**, 031031 (2018).

[60] C.-M. Chung and S. R. White (private communication).

[61] P. Corboz (private communication).

[62] H. J. Schulz, Phys. Rev. Lett. **64**, 1445 (1990).

[63] J. Xu, C.-C. Chang, E. J. Walter, and S. Zhang, J. Phys. Condens. Matter **23**, 505601 (2011).

[64] V. J. Emery, S. A. Kivelson, and H. Q. Lin, Phys. Rev. Lett. **64**, 475 (1990).

[65] Spin-up and spin-down bands are degenerate due to the reflection symmetry around any stripe, namely, a vertical axis with maximum hole density, see Fig. 2. This transformation changes the spin direction of the antiferromagnetic field, namely, the spin-up with the spin-down HF Hamiltonian, that therefore have the same spectrum of eigenvalues.

[66] R. Hlubina, Phys. Rev. B **59**, 9600 (1999).

[67] A. I. Lichtenstein and M. I. Katsnelson, Phys. Rev. B **62**, R9283 (2000).

[68] S. S. Kancharla, B. Kyung, D. Sénéchal, M. Civelli, M. Capone, G. Kotliar, and A.-M. S. Tremblay, Phys. Rev. B **77**, 184516 (2008).

[69] G. Sordi, P. Sémon, K. Haule, and A.-M. S. Tremblay, Phys. Rev. Lett. **108**, 216401 (2012).

[70] X. Chen, J. P. F. LeBlanc, and E. Gull, Phys. Rev. Lett. **115**, 116402 (2015).

[71] A. T. Rømer, T. A. Maier, A. Kreisel, I. Eremin, P. J. Hirschfeld, and B. M. Andersen, Phys. Rev. Res. **2**, 013108 (2020).

[72] K. Ido, T. Ohgoe, and M. Imada, Phys. Rev. B **97**, 045138 (2018).

[73] A. S. Darmawan, Y. Nomura, Y. Yamaji, and M. Imada, Phys. Rev. B **98**, 205132 (2018).

[74] B.-X. Zheng and G. K.-L. Chan, Phys. Rev. B **93**, 035126 (2016).

[75] The low-doped metallic phase presented in Fig. 12 is suggested by the analysis of the striped phases in Fig. 9, which, in turn, is based on mean-field arguments. That is, such analysis just provides hints on the transport properties. A thorough description of the metallic/insulating behavior around the half filling must take into account the behavior of the current-current correlation functions, which is not investigated in this paper.

[76] P. A. Lee, N. Nagaosa, and X.-G. Wen, Rev. Mod. Phys. **78**, 17 (2006).

[77] S. Sorella, Int. J. Mod. Phys. B **05**, 937 (1991).

[78] A. C. Cosentini, M. Capone, L. Guidoni, and G. B. Bachelet, Phys. Rev. B **58**, R14685 (1998).

[79] C.-C. Chang and S. Zhang, Phys. Rev. B **78**, 165101 (2008).

[80] S. Sorella, Phys. Rev. B **91**, 241116(R) (2015).

[81] J. M. Tranquada, B. J. Sternlieb, J. D. Axe, Y. Nakamura, and S. Uchida, Nature (London) **375**, 561 (1995).

[82] H. Shi, C. A. Jiménez-Hoyos, R. Rodríguez-Guzmán, G. E. Scuseria, and S. Zhang, Phys. Rev. B **89**, 125129 (2014).
[83] D. Tahara and M. Imada, J. Phys. Soc. Jpn. **77**, 114701 (2008).
[84] A. Parola, Phys. Rev. B **40**, 7109 (1989).
[85] M. Takahashi, Prog. Theor. Phys. **47**, 69 (1972).
[86] N. D. Mermin and H. Wagner, Phys. Rev. Lett. **17**, 1133 (1966).